SIMCor

In-Silico testing and validation of Cardiovascular IMplantable devices

Call: H2020-SC1-DTH-2018-2020 (Digital transformation in Health and Care)

Topic: SC1-DTH-06-2020 (Accelerating the uptake of computer simulations for testing medicines and medical devices)

Grant Agreement Number: 101017578

Deliverable 9.1

Constitutive vessel model

Due date of delivery: June 30, 2022

Actual submission date: March 31, 2023

Start of the project: 1 January 2021
End date: 31 December 2023

This project has received funding from the European Union's Horizon 2020 research and innovation programmeunder grant agreement N° 101017578

References

Name	SIMCor_D9.1_Constitutive-vessel-model_TUG_31-03-2023
Lead beneficiary	Biotronik SE & CO. KG (BIO)
Author(s)	Malte Rolf-Pissarczyk (TUG), Michele Terzano (TUG)
Dissemination level	Public
Type	Report
Official delivery date	30/06/2022
Date of validation by the WP Leader	31/03/2023
Date of validation by the Coordinator	31/03/2023
Signature of the Coordinator	Jan Bruening Digitally signed by Jan Bruening Date: 2023.03.31 00:49:57 +02'00'

Version log

Issue date	Version	Involved	Comments
03/08/2022	1.1	Malte Rolf-Pissarczyk (TUG), Michele Terzano (TUG)	First draft by TUG
11/08/2022	1.2	Jan Brüning (CHA)	Project Coordinator's review
16/08/2022	1.3	Ingmar Stade (BIO), Valentina Lavezzo (PHI)	Internal review by BIO and PHI
22/08/2022	1.4	Anna Rizzo (LYN), Jan Brüning (CHA)	Final review and formal checking by Project Manager and Project Coordinator
31/08/2022	Final	Jan Brüning (CHA)	Submission by Project Coordinator
20/03/2023	2.1	Malte Rolf-Pissarczyk (TUG), Michele Terzano (TUG)	First draft by TUG
27/03/2023	2.2	Anna Rizzo (LYN), Jan Brüning (CHA)	Project Manager's and Project Coordinator's review
27/03/2023	2.3	Ingmar Stade (BIO), Valentina Lavezzo (PHI)	Internal review by BIO and PHI
27/03/2023	2.4	Anna Rizzo (LYN), Jan Brüning (CHA)	Final review and formal checking by Project Manager and Project Coordinator
31/03/2023	Final	Jan Brüning (CHA)	Submission by Project Coordinator

Executive summary

The deliverable reports all relevant information regarding the development of an enhanced constitutive model to describe the anisotropic material behaviour of the vessel wall, which will be used in combination with the virtual device models for preliminary analyses requiring a reduced computational effort. For this purpose, the constitutive framework of the Holzapfel-Gasser-Ogden model with non-symmetric fibre dispersion is described and subsequently the implementation process in the commercial finite element software ANSYS Mechanical APDL and LS-DYNA is detailed. Two elementary numerical examples are presented to demonstrate the characteristic material behaviour predicted by the model. Initially, the parameters for the Holzapfel-Gasser-Ogden model are derived from existing literature data and then refined using experimental findings from our laboratory. Furthermore, a Bayesian framework is applied in a representative case study to evaluate the uncertainty associated these material parameters.

Table of contents

List of figures

List of tables

Acronyms

Acronym	Full name
TAVI	Transcatheter aortic valve implantation
PAPS	Pulmonary artery pressure sensor
TUG	Graz University of Technology
LYN	Lynkeus
CHA	Charité - Universitätsmedizin Berlin
BIO	Biotronik SE & CO. KG
HGO	Holzapfel-Gasser-Ogden
GST	Generalised structure tensor

Introduction

SIMCor aims to provide manufacturers of cardiovascular implants with a platform for comprehensive in-silico testing and validation of new devices. In particular, simulation of device effects on two representative areas, *transcatheter aortic valve implantation* (TAVI) and *pulmonary artery pressure sensors* (PAPS), is addressed. In order to accurately simulate the implantation of a device, the physical properties of its components, including material, structural, geometric and mechanical features, have to be modelled. In addition, the interaction with the tissue requires an accurate characterisation of mechanical properties and microstructure of the vessel wall, together with the development and validation of an appropriate constitutive model.

The scope of this document is to report all the relevant information regarding the development of a constitutive model to describe the anisotropic material behaviour of the vessel wall. The constitutive modelling framework is presented in *Section Constitutive vessel model* and the implementation process in the commercial finite element software ANSYS Mechanical APDL and LS-DYNA is provided in *Section Implementation*. Two elementary examples, required for the verification of the user-defined constitutive model in ANSYS Mechanical APDL and as an applicative example in LS-DYNA are illustrated in *Section Verification*. Finally, the process of identifying parameters for the anisotropic material model is showcased in *Section Parameter identification*, utilising both data from existing literature and experimental outcomes from our laboratory.

Constitutive vessel model

In this section, we describe the mechanical behaviour of elastic arteries and briefly present the structural arrangement of a healthy arterial wall, which motivated the development of a constitutive vessel model. We then introduce the kinematics underlying the continuum modelling approach, formulate a strain-energy function and derive the expression of the corresponding stress and elasticity tensors.

Mechanical behaviour of arterial walls

The healthy arterial wall consists of a three-layered structure: the inner intimal layer, the medial layer, and the outermost adventitial layer [9]. Each layer presents an interconnected network of collagen fibres, elastin, vascular cells and proteoglycans, with different arrangements, leading to a rather complex mechanical behaviour. The highly organised structural arrangement of collagen in fibre families confers to the healthy arterial wall a typical anisotropic response. Each family is characterised by individual fibres that are distributed symmetrically with respect to a mean fibre direction. Additionally, the individual fibres in each family are not perfectly aligned with the mean direction, but rather they are dispersed around it. Depending on the layer of the arterial wall, the mean fibre orientation and dispersion can be different. For instance, collagen fibres in the media show high alignment, whereas in the intima and adventitia they are significantly dispersed [6].

The constitutive model proposed by Holzapfel et al. [10] is based on the definition of a *generalised structure tensor* (GST), which allows fibres to be represented in a continuum mechanical framework and provides a measure of the fibre distribution. The distribution of fibres is described by a non-symmetric dispersion model based on a pair of von Mises periodic distributions, one for the in-plane behaviour (that is, in the circumferential-axial plane) and a second one for the out-of-plane behaviour. Each layer is assumed to contain two fibre families, symmetrically oriented with respect to the circumferential direction and with same mechanical properties, embedded in a non-collagenous ground matrix. Through an additive split of the strain-energy, the energy stored in the ground matrix is described by an isotropic neo-Hookean model, whereas the strain-energy of the collagen fibres is provided by an anisotropic exponential model enriched by the GST.

Kinematics

Let Ω_0 be the (undeformed) reference configuration and Ω the (deformed) current configuration of the continuous body of interest. We can describe the transformation of a material point $\boldsymbol{X}$ from Ω_0 to Ω using the deformation map χ, such that $\boldsymbol{x} = \chi(\boldsymbol{X})$. Accordingly, the deformation gradient tensor $\mathbf{F}(\boldsymbol{X})$ is defined as $\mathbf{F}(\boldsymbol{X}) = \partial\chi(\boldsymbol{X})/\partial\boldsymbol{X}$ [8]. Furthermore, the reference orientations of two fibre families are represented by the in-plane unit vectors $\boldsymbol{M}_4$ and $\boldsymbol{M}_6$, with $\|\boldsymbol{M}_4\| = \|\boldsymbol{M}_6\| = 1$, and by unit out-of-plane vectors $\boldsymbol{M}_\mathrm{n}$.

Arteries, like many others biological tissues, are known to behave as almost incompressible materials, for which we introduce the well-known constraint on the determinant of the deformation gradient $J = \det(\mathbf{F}) \equiv 1$. However, for computational purposes, it might be beneficial to introduce a multiplicative split of the deformation gradient into volumetric and deviatoric parts. Accordingly, the dilational part of the the deformation gradient appears as $J^{1/3}\mathbf{I}$, leaving a purely distortional part $\bar{\mathbf{F}} = J^{-1/3}\mathbf{F}$, with $\mathbf{I}$ the second-order unit tensor. The symmetric right and left Cauchy-Green tensors, which represent the deformation measures in the reference and current configurations, are defined as follows

$$\mathbf{C} = \mathbf{F}^\mathrm{T} \cdot \mathbf{F}, \quad \bar{\mathbf{C}} = J^{-2/3}\mathbf{C}; \tag{1}$$

$$\mathbf{b} = \mathbf{F} \cdot \mathbf{F}^\mathrm{T}, \quad \bar{\mathbf{b}} = J^{-2/3}\mathbf{b}. \tag{2}$$

The isotropic hyperelastic response is characterised by the following strain invariants

$$I_1 = \mathbf{C} : \mathbf{I} = \mathbf{b} : \mathbf{I}, \quad \bar{I}_1 = J^{-2/3} I_1; \tag{3}$$

$$I_2 = J^2 \mathbf{C}^{-1} : \mathbf{I} = J^2 \mathbf{b}^{-1} : \mathbf{I}, \quad \bar{I}_2 = J^{-4/3} I_2. \tag{4}$$

Anisotropic hyperelasticity requires the definition of additional invariants related to the deformation of the fibre families. Specifically, we here consider the following invariants

$$I_i = \mathbf{C} : \boldsymbol{M}_i \otimes \boldsymbol{M}_i, \quad i = 4, 6\,, \tag{5}$$

where the volumetric-deviatoric split is not applied since it is known to give rise to nonphysical behaviour in anisotropic hyperelasticity [7].

As previously mentioned, fibre dispersion is included in the model through the GST concept, defined here by the following symmetric second-order tensor [10]

$$\mathbf{H}_i = A\mathbf{I} + B\boldsymbol{M}_i \otimes \boldsymbol{M}_i + (1 - 3A - B)\boldsymbol{M}_\mathrm{n} \otimes \boldsymbol{M}_\mathrm{n}, \quad i = 4, 6\,, \tag{6}$$

where $A = 2\kappa_\mathrm{op}\kappa_\mathrm{ip}$ and $B = 2\kappa_\mathrm{op}(1 - 2\kappa_\mathrm{ip})$ are parameters related to the in-plane and out-of-plane fibre dispersions κ_ip and κ_op [10]. We can then define the generalized strain invariants $I_4^\star$ and $I_6^\star$ as

$$I_i^\star = \mathbf{C} : \mathbf{H} = AI_1 + BI_i + (1 - 3A - B)I_\mathrm{n}, \quad i = 4, 6\,, \tag{7}$$

with $I_\mathrm{n} = \mathbf{C} : (\boldsymbol{M}_\mathrm{n} \otimes \boldsymbol{M}_\mathrm{n})$.

Strain-energy function

With the assumption of anisotropic material behaviour described by the GST proposed in (6), a strain-energy function can be formulated in terms of the invariants and pseudo-invariants of the right Cauchy-Green strain tensor

$$\Psi = \Psi(I_1, I_2, I_4^\star, I_6^\star) - p(J - 1), \tag{8}$$

where p serves an indeterminate Lagrange multiplier to enforce the material incompressibility. However, when the multiplicative split of the deformation is adopted, the strain-energy function presents the following additive form

$$\Psi = \Psi_\mathrm{iso}(\bar{I}_1, \bar{I}_2) + \hat{\Psi}(I_4^\star, I_6^\star) + U(J), \tag{9}$$

where:

- $\Psi_\mathrm{iso}(\bar{I}_1, \bar{I}_2)$ is the isochoric isotropic part associated with volume-preserving deformations. In this model, a neo-Hookean strain energy, which is a linear function of the first strain invariant, is adopted

  $$\Psi_\mathrm{iso}(\bar{I}_1) = \frac{\mu}{2}(\bar{I}_1 - 3), \tag{10}$$

  with μ the shear modulus of the non-collagenous ground matrix material.

- $\hat{\Psi}(I_4^\star, I_6^\star)$ is the anisotropic part. In this model, we consider two symmetric fibre families with identical structural and mechanical parameters, with each fibre family having an exponential strain-energy function expressed in terms of the generalized pseudo-invariants. The form of the anisotropic part of the strain-energy function is [10]

  $$\hat{\Psi}(I_4^\star, I_6^\star) = \sum_{i=4,6} \frac{k_1}{2k_2}\{\exp[k_2(I_i^\star - 1)^2] - 1\}, \tag{11}$$

where k_1 is the shear modulus of the fibres and k_2 is a dimensionless parameter controlling the strain-stiffening behaviour. An important point concerns the behaviour under compression. It is often assumed that fibres can only bear tensile loads and their contribution to the overall mechanical response should be neglected when they are compressed. Therefore, a tension-compression switch is introduced in the formulation based on the invariants I_i, such that the contribution of the fibre family to the strain-energy (11) is neglected when $I_i \leq 1$ [11]. Besides, this switch also ensures the poly-convexity requirements of the strain-energy function [6].

- $U(J)$ is the term associated with volume-changing deformations, usually provided by a convex function of the determinant J. In this model, the following form is chosen

  $$U(J) = \frac{K}{2}(J-1)^2, \tag{12}$$

  with K the material bulk modulus, which should be here understood as a penalty parameter to enforce incompressibility.

Stress tensor

Following the additive decomposition of the strain-energy function presented in (9), the Cauchy stress tensor for the modified nearly-incompressible formulation is defined by

$$\boldsymbol{\sigma} = \boldsymbol{\sigma}_{\mathrm{iso}} + \sum_{i=4,6} \boldsymbol{\sigma}_i + \boldsymbol{\sigma}_{\mathrm{vol}}, \tag{13}$$

where:

- $\boldsymbol{\sigma}_{\mathrm{iso}}$ is the isotropic isochoric stress tensor defined as

  $$\boldsymbol{\sigma}_{\mathrm{iso}} = \mathbb{p} : (2J^{-1}\frac{\partial \boldsymbol{\Psi}_{\mathrm{iso}}}{\partial \bar{\mathbf{b}}}\bar{\mathbf{b}}) = \mathbb{p} : \bar{\boldsymbol{\sigma}}, \tag{14}$$

  where we have introduced the projection tensor $\mathbb{p} = \mathbb{I} - \frac{1}{3}\mathbf{I} \otimes \mathbf{I}$, with $\mathbb{I}$ the fourth-order identity tensor. The fictitious stress tensor $\bar{\boldsymbol{\sigma}}$ can be written as

  $$\bar{\boldsymbol{\sigma}} = J^{-1}\psi_1 \bar{\mathbf{b}}, \tag{15}$$

  with stress coefficient $\psi_1 = 2\,\partial\Psi_{\mathrm{iso}}(\bar{I}_1)/\partial\bar{I}_1$. For the form introduced in (10), the expression is reported in *Table* 1.

- $\boldsymbol{\sigma}_i$ is the anisotropic stress tensor defined in each collagen fibre family, given by

  $$\boldsymbol{\sigma}_i = J^{-1}\psi_i \mathbf{h}_i, \quad i = 4, 6\,, \tag{16}$$

  where we have introduced the push-forward of the structure tensor $\mathbf{h}_i = \mathbf{F} \cdot \mathbf{H}_i \cdot \mathbf{F}^{\mathrm{T}}$ and the stress coefficients $\psi_i = 2\,\partial\hat{\Psi}/\partial I_i^\star$ [6]. For the form introduced in (11), the expression is reported in *Table* 1.

- $\boldsymbol{\sigma}_{\mathrm{vol}}$ is the volumetric stress tensor defined as

  $$\boldsymbol{\sigma}_{\mathrm{vol}} = p\mathbf{I}, \tag{17}$$

  with the volumetric stress coefficient $p = dU/dJ$. For the strain-energy introduced in (12), the expression is provided in *Table* 1.

Elasticity tensor

The implementation of a nonlinear material model in an implicit finite element code is based on the linearisation of constitutive equations and requires the definition of an elasticity tensor. Following the modified nearly-incompressible formulation, we have an additive representation of the spatial elasticity tensor as reported below

$$\mathbb{c} = \mathbb{c}_{\text{iso}} + \sum_{i=4,6} \mathbb{c}_i + \mathbb{c}_{\text{vol}}, \tag{18}$$

where:

- $\mathbb{c}_{\text{iso}}$ is the isotropic isochoric elasticity tensor defined as [8]

  $$\mathbb{c}_{\text{iso}} = \mathbb{p} : \bar{\mathbb{c}} : \mathbb{p} + \frac{2}{3}\text{tr}(\bar{\boldsymbol{\sigma}})\,\mathbb{p} - \frac{2}{3}(\mathbf{I} \otimes \boldsymbol{\sigma}_{\text{iso}} + \boldsymbol{\sigma}_{\text{iso}} \otimes \mathbf{I}), \tag{19}$$

  and the fictitious elasticity tensor $\bar{\mathbb{c}}$ can be written as

  $$\bar{\mathbb{c}} = J^{-1}\psi_{11}(\bar{\mathbf{b}} \otimes \bar{\mathbf{b}}), \tag{20}$$

  with the elasticity coefficient $\psi_{11} = 4\,\partial^2\Psi_{\text{iso}}/\partial\bar{I}_1\partial\bar{I}_1$. For the form introduced in (10), the expression is reported in *Table* 1.

- $\mathbb{c}_i$ is the anisotropic contribution to the elasticity tensor for each collagen fibre family, given by [6]

  $$\mathbb{c}_i = J^{-1}\psi_{ii}(\mathbf{h}_i \otimes \mathbf{h}_i), \quad i = 4, 6\,, \tag{21}$$

  with the elasticity coefficients $\psi_{ii} = 4\,\partial^2\hat{\Psi}/\partial I_i^\star \partial I_i^\star$. For the form introduced in (11), the expression is reported in *Table* 1.

- $\mathbb{c}_{\text{vol}}$ is the volumetric elasticity tensor defined as

  $$\mathbb{c}_{\text{vol}} = \tilde{p}\mathbf{I} \otimes \mathbf{I} - 2p\mathbb{I}, \tag{22}$$

  with the volumetric elasticity coefficient $\tilde{p} = p + J dp/dJ$. For the strain-energy introduced in (12), the expression is provided in *Table* 1.

Variable	**Expression**
Isotropic isochoric strain-energy function	$\Psi_{\text{iso}}(\bar{I}_1) = \frac{\mu}{2}(\bar{I}_1 - 3)$
Isotropic isochoric stress coefficient, see (15)	$\psi_1 = \mu$
Isotropic isochoric elasticity coefficient, see (20)	$\psi_{11} = 0$
Anisotropic strain-energy function	$\hat{\Psi}(I_4^\star, I_6^\star) = \sum_{i=4,6} \frac{k_1}{2k_2}\{\exp[k_2(I_i^\star - 1)^2] - 1\}$
Anisotropic stress coefficient, see (16)	$\psi_i = k_1(I_i^\star - 1)\exp[k_2(I_i^\star - 1)^2], \quad i = 4,6$
Anisotropic elasticity coefficient, see (21)	$\psi_{ii} = k_1[1 + 2k_2(I_i^\star - 1)^2]\exp[k_2(I_i^\star - 1)^2], \quad i = 4,6$
Volumetric strain-energy function	$U(J) = \frac{K}{2}(J-1)^2$
Volumetric stress coefficient, see (17)	$p = K(J-1)$
Volumetric elasticity coefficient, see (22)	$\tilde{p} = K(J-1) + JK$

Table 1: Implementation of anisotropic constitutive equations with the modified nearly-incompressible formulation.

Implementation

The constitutive model described above is implemented into the commercial finite element software ANSYS Mechanical APDL and LS-DYNA. This section provides details about the definition of the required material parameters and options.

ANSYS Mechanical APDL

Implementation of the constitutive model

ANSYS Mechanical APDL material library includes several hyperelastic constitutive models and provides options for implementing incompressible and nearly-incompressible formulations. However, the software does not provide an in-built material definition of the constitutive model proposed by [10] and presented in *Section Constitutive vessel model*. Therefore, a user material must be implemented through the subroutine `UserMat`. The `UserMat` is a user-programmable feature for developing a generic isothermal constitutive model through a user-defined FORTRAN code. With respect to hyperelastic material models, it is convenient to formulate the constitutive equations in the total form, which directly employs the deformation gradient passed in to the user-subroutine. The subroutine is then called at each integration point of the elements during the solution phase.

The user material is defined following the constitutive equations presented in *Section Constitutive vessel model*. Specifically, the nearly-incompressible formulation shown in (9) is implemented, with the volumetric strain-energy expressed by

$$U(J) = \frac{1}{d}(J-1)^2, \tag{23}$$

where $d = 2/K$ is the material incompressibility parameter. Notice that by setting $d = 0$ the material is fully incompressible. For compatibility with the simplified vessel model implemented in *Deliverable 8.3 - Constitutive vessel model (TUG, M20)*, the isotropic isochoric strain-energy function is provided by the following exponential form

$$\Psi_{\mathrm{iso}}(\bar{I}_1) = \frac{\mu}{2b}\{\exp[b(\bar{I}_1 - 3)] - 1\}, \tag{24}$$

where the dimensionless parameter b accounts for the strain-stiffening of the material. By taking $b \to 0$, one obtains $\exp[b(\bar{I}_1 - 3)] \approx b(\bar{I}_1 - 3) + 1$, such that the neo-Hookean strain-energy (10) is recovered [13].

UserMat implementation

The constitutive model is implemented in a FORTRAN code, which is made available to the consortium members as supplementary material (google.drive).

The following subroutines are called from the main ANSYS Mechanical APDL subroutine `UserMat`:

- `usermat3D`: subroutine providing the stress in the current configuration (symmetric Cauchy stress tensor `stress`), the Eulerian elasticity tensor (material Jacobian in terms of the Jaumann rate of the Kirchhoff stress `dsdePl`) and the elastic strain energy `sedEl`. Suitable for 3D, axisymmetric and plane strain elements.Additional subroutines are included as follows:
  - `estressI1I2`: subroutine computing the isotropic isochoric (fictitious) part of the Cauchy stress tensor;
  - `estressI1I4In`: subroutine computing the anisotropic part of the Cauchy stress tensor;

  - `etensI1I2`: subroutine computing the isotropic isochoric (fictitious) part of the spatial elasticity tensor;
  - `etensI1I4In`: subroutine computing the anisotropic part of the spatial elasticity tensor;
  - `devetens`: subroutine computing the deviatoric part of the spatial elasticity tensor.

In addition, the following user-defined utility subroutines are called throughout the code:

- `identity`: subroutine providing the identity tensor and its dyadics;
- `voigt2`: subroutine transforming a symmetric second-order tensor in matrix form into Voigt's notation;
- `bdet`: subroutine computing the determinant of a (3x3) matrix;
- `dyad6`: subroutine computing the dyadic product of two symmetric second-order tensors in Voigt's notation;
- `sym4tens66`: subroutine computing the symmetrised square dyadic product of two symmetric second-order tensors in Voigt's notation;
- `contract66`: subroutine computing the double contraction of two fourth-order tensors with major symmetries in Voigt's notation.

We recall that tensors should be stored in matrix format using Voigt's notation; to give an example, the second-order Cauchy stress tensor is represented as

$$[\boldsymbol{\sigma}] = [\sigma_{11}\ \sigma_{22}\ \sigma_{33}\ \sigma_{12}\ \sigma_{23}\ \sigma_{13}]^{\mathrm{T}}. \tag{25}$$

Required input

Material models in ANSYS Mechanical APDL are specified through the command TB, followed by the command TBDATA to pass in the material parameters. A summary of the parameters and keywords required for the user material is reported in *Table* 2.
Additional parameters need to be passed in to the user-defined subroutine through the script `kpars_umat.for`. The required parameters include:

- `aloc`: flag for material orientation. Set `aloc=1,2,3`, where the number is related to the basis vector $\boldsymbol{E}_A$ identifying the local circumferential direction in the reference configuration;
- `ncf`: number of fibre families, with `ncf` ≤ 2;
- `parv`: Voigt's ordering convention. In ANSYS Mechanical APDL, `parv=2` must be chosen to specify that the shear components of symmetric second-order tensors are ordered as `{12,23,13}`.

Software quality assurance

The user-material subroutine here developed is provided as FORTRAN source code (FORTRAN 90 or later) and needs to be compiled by using a proper FORTRAN compiler. All the results provided as benchmark problems were obtained by running ANSYS Mechanical APDL 2021 R1 and Intel Fortran Compiler 2022.0.2, included in the Intel oneAPI Base and Intel oneAPI HPC Toolkits, combined with Microsoft Visual Studio 2019. The user-material subroutine has been linked into a Dynamic-link Library, as specified in the software documentation [2]. To the best of the authors' knowledge, there are no known compiler-related issues that could affect the application of the implemented user-defined subroutine.

Definition	Keyword	Value
TB command		
Material model type	Lab	USER
Data table specification	TBOPT [1]	-
Number of data points	NPTS	9
TBDATA command		
Material incompressibility parameter d	C1	t.b.d.
Shear modulus μ	C2	t.b.d.
Material strain-stiffening parameter b [2]	C3	t.b.d.
Angle of 1st fibre family α_4 [3]	C4	t.b.d.
In-plane dispersion parameter $\kappa_{\text{ip}} \in [0, 1]$	C5	t.b.d.
Out-of-plane dispersion parameter $\kappa_{\text{op}} \in [0, 1/2]$	C6	t.b.d.
Fibre shear modulus k_1	C7	t.b.d.
Fibre strain-stiffening parameter k_2	C8	t.b.d.
Angle of 2nd fibre family α_6 [3]	C9	t.b.d.

Table 2: Summary of material parameters and keywords required for the implementation of the proposed constitutive model with the `UserMat` *subroutine in ANSYS Mechanical APDL.*

[1] *If not specified, the default value of TBOPT is NONLINEAR. However, if the material behaviour is considered fully incompressible, a mixed element formulation should be selected by setting TBOPT=MXUP.*

[2] *The neo-Hookean strain-energy function is implemented by taking $b \to 0$.*

[3] *The fibre orientation is defined by the angle (in degrees) with respect to the local circumferential direction, measured anticlockwise.*

LS-DYNA

Implementation of the constitutive model

LS-DYNA offers a vast material library with several constitutive models suitable for isotropic hyperelastic response. With specific reference to soft biological tissues, the material identified by the code *MAT_295 provides a modular framework for incompressible or nearly-incompressible, isotropic and anisotropic hyperelastic constitutive models [3]. Different options are available, which are specified by so-called material cards. In this section, this material will be employed to implement the proposed anisotropic constitutive model. For user convenience, a short theoretical summary with the original notation employed in the software documentation is presented here.

The general form of the strain-energy function implemented in *MAT_295 is analogous to the one described in *Section Constitutive vessel model*; for better clarity, we keep here the original notation employed in the software user manual [3]. Adopting the modified nearly-incompressible formulation, the isotropic strain-energy is written as

$$\Psi = \Psi_{\text{iso}}(\bar{I}_1) + \hat{\Psi}(\mathbf{F}, \mathbf{H}_j) + U(J). \qquad (26)$$

Specifically, the isochoric isotropic part is expressed by

$$\Psi_{\mathrm{iso}}(\bar{I}_1) = \frac{k_1}{2k_2}\{\exp[k_2(\bar{I}_1 - 3)] - 1\}, \tag{27}$$

where $k_1 \equiv \mu$ is the material shear modulus and $k_2 \equiv b$ is the dimensionless parameter accounting for strain-stiffening. We recall that by taking $k_2 \equiv b \to 0$ the neo-Hookean strain-energy (10) is recovered [13].

The anisotropic strain-energy function is defined in LS-DYNA as [3]

$$\hat{\Psi}(\mathbf{F}, \mathbf{H}_j) = \sum_{j=1}^{\mathrm{nf}} \chi_j \frac{k_{1j}^{\mathrm{A}}}{2k_{2j}^{\mathrm{A}}}[\exp(k_{2j}^{\mathrm{A}} E_j^2) - 1], \tag{28}$$

where $j \in [1, \mathrm{nf}]$ denotes the single fibre family, nf is the number of fibre families and $E_j = \mathbf{C} : \mathbf{H}_j - 1$ is a Green-Lagrange strain-like quantity associated to the generalized structure tensor $\mathbf{H}_j$ [6]. Notice that by assuming two fibre families ($\mathrm{nf} = 2$) with same material parameters, and considering the following transformation of indices $j = 1 \to i = 4, j = 2 \to i = 6$, the strain-energy function in (28) is equivalent to (11). The tension-compression switch is here enforced through the parameter χ_j, such that compressed fibres are excluded, $\chi_j = 0$, when the fibre stretch $\lambda_j \leq 1$. This is consistent with the original formulation, which implements the switch based on the fibre invariant $I_j = \lambda_j^2 \leq 1$ [11]. A summary of the parameters and keywords required for the implementation of the material is reported in *Table* 3.

Basics (Card 1)		
Definition	**Keyword**	**Value**
Material identification	MID	1
Mass density [1]	ρ	1.0
Material axes option	AOPT	2

Isotropic part (Card 2)			***Isotropic part (Card 2.1c)***		
Definition	**Keyword**	**Value**	**Definition**	**Keyword**	**Value**
Module title	TITLE	ISO	Holzapfel-Ogden modulus	k_1	t.b.d.
Type of isotropic model [3]	ITYPE	-3	Holzapfel-Ogden constant	k_2	$\to 0$
Volumetric coefficient	β	0.0			
Poisson's ratio	ν	t.b.d.			

Anisotropic part (Card 3)		
Definition	**Keyword**	**Value**
Module title	TITLE	ANISO
Type of anisotropic model [4]	ATYPE	+1
Type of interaction	INTYPE	0
Number of fibre families	nf	2

Anisotropic part (Card 3.1) [5]			***Anisotropic part (Card 3.2a)*** [5]		
Definition	**Keyword**	**Value**	**Definition**	**Keyword**	**Value**
Mean fibre orientation [6]	θ	t.b.d.	Type of fibre model [4]	FTYPE	1
First GST parameter	A	t.b.d.	Curve ID	FCID	0
Second GST parameter	B	t.b.d.	HGO modulus	k_1^{A}	t.b.d.
			HGO constant	k_2^{A}	t.b.d.

*Table 3: Summary of material parameters and keywords for LS-DYNA material model *MAT_295. The combination presented here implements a nearly-incompressible, anisotropic material behaviour with an isochoric neo-Hookean strain-energy function and the anisotropic strain-energy function proposed by Holzapfel et al. [10].*

[1] *Mass density is not relevant for the implicit algorithm.*

[3] *ITYPE=-3 implements the isotropic isochoric exponential strain-energy function as in* (27).

[4] *The combination of ATYPE=+1 and FTYPE=1 implements the anisotropic exponential strain-energy function as in* (28).

[5] *These cards must be defined for each fibre family.*

[6] *The fibre orientation* $\theta_j \equiv \alpha_i$ *is defined by the angle (in degrees) with respect to the local circumferential direction, measured anticlockwise.*

Material orientation

For the correct formulation of an anisotropic material model, definition of the material orientation is of primary importance. In the following, we present the theoretical framework and related computational procedures, needed to implement the material orientation in ANSYS Mechanical APDL and LS-DYNA.

Global and local bases

In general, material orientation is defined by a local reference basis $\boldsymbol{E}_I$, $I = 1, 2, 3$, which can be specified through a rotation of the global basis $\boldsymbol{G}_I$, such that $\boldsymbol{E}_I = \mathbf{Q}_{IJ}\boldsymbol{G}_J$, where $Q_{IJ} = \boldsymbol{E}_I \cdot \boldsymbol{G}_J$ is a proper orthogonal tensor [8]. The form of the structure tensor presented in (6) assumes that the unit fibre orientation $\boldsymbol{M}_i$ is defined with respect to the local basis vectors $\boldsymbol{E}_1, \boldsymbol{E}_2$ and $\boldsymbol{E}_3$, forming a basis aligned to the local circumferential, axial and radial directions of a cylindrical coordinate system (*Figure* 1).
We suggest two possible strategies for a correct implementation of an anisotropic material model. The most straightforward one is to formulate the constitutive equations directly in the local reference basis, such that, for instance, a material second-order tensor is expressed as $\mathbf{T} = T_{IJ}\boldsymbol{E}_I \otimes \boldsymbol{E}_J$. In the current configuration, the local basis follows the rotation of the material defined by $\mathbf{R}$, such that the corresponding spatial second-order tensor is defined by $\mathbf{t} = t_{ij}\boldsymbol{e}_i \otimes \boldsymbol{e}_j$. The current unit vectors $\boldsymbol{e}_i$ defines the so-called corotational basis of the material, with $\boldsymbol{e}_i = \mathbf{R} \cdot \boldsymbol{E}_I$. The second approach operates within the global basis and applies an element-wise rotation to the structure tensor. Accordingly, the structure tensor (6) in the global basis is expressed as $\mathbf{H}^{\mathrm{G}} = \mathbf{Q}^{\mathrm{T}} \cdot \mathbf{H}^{\mathrm{E}} \cdot \mathbf{Q}$, where the superscripts $^{\mathrm{G,E}}$ identify the structure tensor expressed in the global and local reference bases, respectively. We have here omitted the subscripts of the fibre family for the sake of clarity.
Finally, we recall that a transformation between spatial tensors expressed in the different bases is possible through the following relationship and its inverse

$$\mathbf{t}^{\mathrm{G}} = (\mathbf{Q} \cdot \mathbf{R}) \cdot \mathbf{t}^{\mathrm{e}} \cdot (\mathbf{Q} \cdot \mathbf{R})^{\mathrm{T}}, \tag{29}$$

where the superscript $^{\mathrm{e}}$ identifies the tensor in the corotational basis.

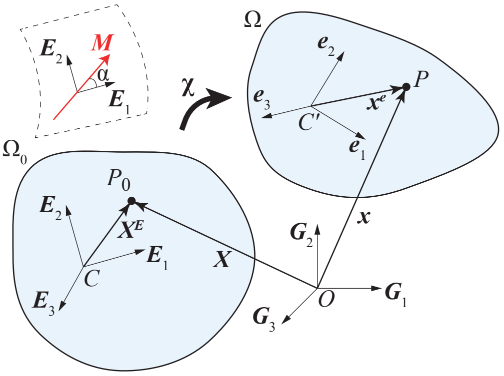

Figure 1: Illustration of the global, local and corotational bases involved in the definition of material orientation in an anisotropic model. The red arrow shows the mean orientation of a single fibre family.

Computational procedure

Whenever the geometry is complex, constructing a physically meaningful local material orientation to employ anisotropic material models is not straightforward. Common approaches involve solving multiple auxiliary Laplace problems with user-specified boundary conditions, such that the local orientations of the material are provided by the normalised flux vectors. In the implementation proposed here, we have chosen a heat transfer problem, such that the local orientations are uniquely obtained from the solution of a pair of steady-state heat transfer analyses. The governing equations are summarised by

$$\begin{aligned} \Delta\Phi_k &= 0 \quad \text{in} \quad \Omega_0, && (30a)\\ \Phi_k &= 0 \quad \text{on} \quad \Gamma_{\text{in}}, && (30b)\\ \Phi_k &= \bar{\Phi}_k \quad \text{on} \quad \Gamma_{\text{out}}, && (30c)\\ \boldsymbol{N}\cdot\nabla\Phi_k &= 0 \quad \text{on} \quad \Gamma_0, && (30d) \end{aligned}$$

where the auxiliary scalar Φ_k represents a temperature, with $k = l, n$ for the longitudinal and radial directions, respectively. The symbols ∇ and Δ denote the gradient and Laplacian operators, respectively. In (30), boundary conditions of the first type are imposed as prescribed temperatures, such that at the the inlet surface Γ_{in} the temperature is set to zero, whereas at the outlet Γ_{out} the temperature is set to a value $\bar{T}_k > 0$. Note that the value of the temperature field variable is not relevant, provided that a sufficiently large gradient is generated in the volume. A boundary condition of the second type at the exterior boundary Γ_0 ensures a heat flux in the longitudinal or radial direction, where $\boldsymbol{N}$ identifies the unit normal to the respective surface.

The local basis vectors are computed from the heat fluxes. Solving the Laplace problem in longitudinal direction $(i = l)$ provides $\mathbf{E}_2$ and in radial direction $(i = n)$ provides $\mathbf{E}_3$. Then, the circumferential direction $\mathbf{E}_1$ can be derived from $\mathbf{E}_2$ and $\mathbf{E}_3$ using basic vector algebra. By applying normalisation, the basis vectors are

$$\begin{aligned} \mathbf{E}_2 &= \frac{\nabla\Phi_l}{||\nabla\Phi_l||},\\ \mathbf{E}_3 &= \frac{\nabla\Phi_n}{||\nabla\Phi_n||},\\ \mathbf{E}_1 &= \mathbf{E}_2 \times \mathbf{E}_3. \end{aligned} \tag{31}$$

Finally, a Procrustes analysis is performed to check orthogonality of the local basis and perform a correction if this is not the case. The orthogonal matrix $Q = M(M^TM)^{-1/2}$ is defined, with

$$M = \begin{bmatrix} \mathbf{E}_{1_1} & \mathbf{E}_{2_1} & \mathbf{E}_{3_1} \\ \mathbf{E}_{1_2} & \mathbf{E}_{2_2} & \mathbf{E}_{3_2} \\ \mathbf{E}_{1_3} & \mathbf{E}_{2_3} & \mathbf{E}_{3_3}, \end{bmatrix} \tag{32}$$

Keep in mind that the entire process must be carried out prior to conducting any mechanical analysis that applies the anisotropic material model. Since the basis vectors obtained depend only on the geometry, the heat transfer analysis needs to be repeated only when the geometry or mesh are changed. The computational procedure is detailed below for both ANSYS Mechanical APDL and LS-DYNA and is made available to the consortium members as supplementary material (google.drive).

ANSYS Mechanical APDL implementation

This section explains how to define a steady-state heat transfer analysis, how to retrieve the local basis vectors from the heat fluxes and how to specify the local material orientation in the subsequent mechanical analysis in ANSYS Mechanical APDL.

The implementation of the steady-state heat transfer analysis in ANSYS Mechanical APDL and the related keywords are summarised in Table 4.

Firstly, a proper element type for thermal analysis should be specified through the command ET. The material thermal behaviour should be specified through the command MP, by setting the thermal density,

Definition	**Keyword**	**Value**
ET command		
Element type	ET	278[1]
MP command[2]		
Specific heat	C	1
Mass density	ìDENS	1
Thermal conductivity	KXX, KYY, KZZ	1
ANTYPE command		
Analysis type	ANTYPE	0[3]
D command		
Node or node set	NODE	t.b.d.
Degree-of-freedom label	Lab	TEMP
Value	VALUE	0
IC command		
Node or node set	NODE	t.b.d.
Degree-of-freedom label	Lab	TEMP
Value	VALUE	0

Table 4: Summary of material parameters and keywords for ANSYS Mechanical APDL steady-state heat transfer analysis.
[1] Three dimensional 8-node thermal solid element.
[2] Linear material definition. Material parameters can be set to unity since only the direction of the heat flux is of interest.
[3] Steady-state heat transfer analysis.

specific heat, and thermal conductivity. Since the purpose of the thermal analysis is to obtain the directions of the heat flux, these parameters can be set to unity. Then, a thermal analysis must be specified through the command ANTYPE. Specifically, ANTYPE=0 activates a steady-state heat transfer analysis [1]. Boundary conditions, as defined in (30), must be specified on the relevant parts of the model, which can be conveniently grouped in node sets. The command D, with label TEMP for the degree-of-freedom, is used to prescribe temperatures, as defined in (30)b-c. Finally, the output of the thermal analysis is written to the database. Specifically, the thermal flux vector TF is accessed in the subsequent post-processing step. A Matlab script is used for this purpose.

The heat flux extracted at each node of the model is stored as a vector with components expressed in the global basis. Firstly, the script computes the heat flux at the centroid of each element. Then, by normalising the fluxes, the local longitudinal orientation ($\mathbf{E}_2 = \nabla\Phi_l/||\nabla\Phi_l||$) and local radial orientation ($\mathbf{E}_3 = \nabla\Phi_n/||\nabla\Phi_n||$) are determined. The local circumferential orientation is obtained through the cross-product $\mathbf{E}_1 = (\mathbf{E}_2 \times \mathbf{E}_3)$. An example of the basis vectors obtained for an axisymmetric geometry is shown in *Figure* 2.

For the definition of the material orientation in a user-defined material model, ANSYS Mechanical ADPL offers multiple options. Using the command LOCAL, an element-wise local coordinate system

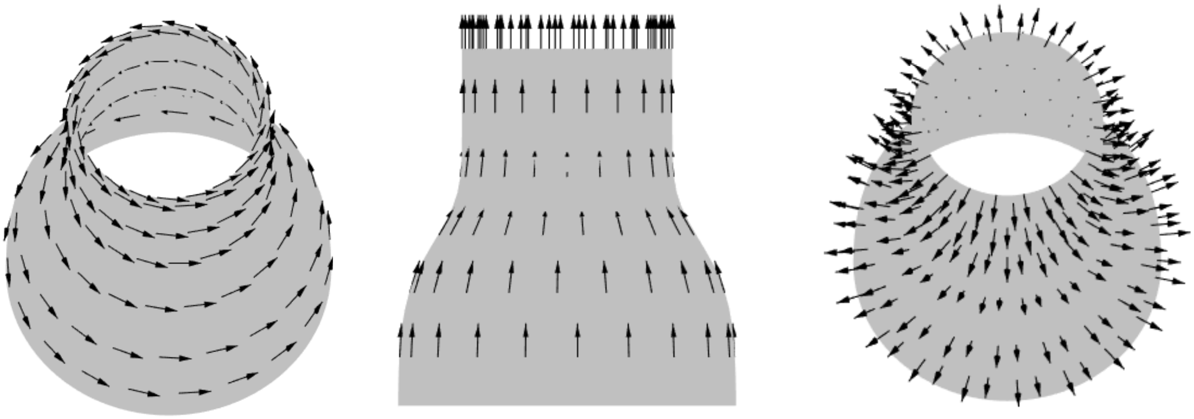

Figure 2: (a) Local circumferential, (b) longitudinal and (c) radial reference directions in a generic axisymmetric geometry.

can be defined by specifying origin location and orientation angles with respect to the global basis (in degrees). According to the software documentation [1], the orientation angles should describe three rotations about the local reference basis vectors.

LS-DYNA implementation

This section explains how to define a steady-state heat transfer analysis, how to retrieve the local basis vectors from the heat fluxes and how to specify the local material orientation in the subsequent mechanical analysis in LS-DYNA.

The implementation of the steady-state heat transfer analysis in LS-DYNA and the related keywords are summarised in Table 5.

Firstly, a thermal analysis must be specified through the keyword *CONTROL_THERMAL_SOLVER. Specifically, ATYPE=0 activates a steady-state heat transfer analysis, PTYPE=0 selects a linear thermal problem type and the option SOLVER=11 activates the default direct solver [3]. Then, the material thermal behaviour should be specified through the material card *MAT_THERMAL_ISOTROPIC, by setting the thermal density, specific heat, and thermal conductivity. Since the purpose of the thermal analysis is to obtain the directions of the heat flux, these parameters can be set to unity. Boundary conditions, as defined in (30), must be specified on the relevant parts of the model. The keyword *BOUNDARY_TEMPERATURE_SET is used to define boundary conditions of the first type in the heat transfer problem, as defined in (30)b-c.

The output of the thermal analysis is then accessed for the subsequent post-processing step, using the keyword *DATABASE_TPRINT. A Python script is used for this purpose. The heat flux is extracted at each node of the model and stored as vector with components expressed in the global basis. Firstly, the script computes the heat flux at the centroid of each element. Then, by normalising the fluxes, the local longitudinal orientation ($\mathbf{E}_2 = \nabla\Phi_l/||\nabla\Phi_l||$) and local radial orientation ($\mathbf{E}_3 = \nabla\Phi_n/||\nabla\Phi_n||$) are obtained The local circumferential orientation is obtained through the cross-product $\mathbf{E}_1 = (\mathbf{E}_2 \times \mathbf{E}_3)$. Finally, the basis vectors $\boldsymbol{E}_1$ and $\boldsymbol{E}_2$ are extracted to be imported and used in an LS-DYNA mechanical analysis. An example of the basis vectors obtained for an axisymmetric geometry is shown in *Figure* 3. In this case, the global basis is the canonical Cartesian coordinate system X, Y, Z. For the definition of the material orientation in an anisotropic material model, LS-DYNA offers multiple options, which can be activated in the anisotropic card of the material model *MAT_295 through the keyword AOPT [3]. We choose to specify the local reference basis $\boldsymbol{E}_I$ of each element by directly including it in the element definition. In the material card (*Table* 3), the keyword AOPT=2 specifies a local basis that coincides

Definition	**Keyword**	**Value**
***MAT_THERMAL_ISOTROPIC** [1]		
Thermal material identification	TMID	1
Thermal density	TRO	1
Specific heat	HC	1
Thermal conductivity	TC	1
***BOUNDARY_TEMPERATURE_SET**		
Node or set ID [2]	NID	t.b.d.
Temperature, specification.	TLCID	
Temperature, curve multiplier	TMULT	
***INITIAL_TEMPERATURE_SET**		
Node set ID [2]	NSID	
Temperature at node set	TEMP	0
***CONTROL_THERMAL_SOLVER**		
Thermal analysis type	ATYPE	0
Thermal problem type	PTYPE	0
Thermal analysis solver type	SOLVER	11
***DATABASE_TPRINT**		
Time interval between outputs	DT	
Flag for binary output	BINARY	3

Table 5: Summary of material parameters and keywords for LS-DYNA steady-state heat transfer analysis.
[1] *Material parameters can be set to unity since only the direction of the heat flux is of interest.*
[2] *Node sets at which boundary conditions are prescribed can be identified through the keyword *SET_NODE_LIST.*

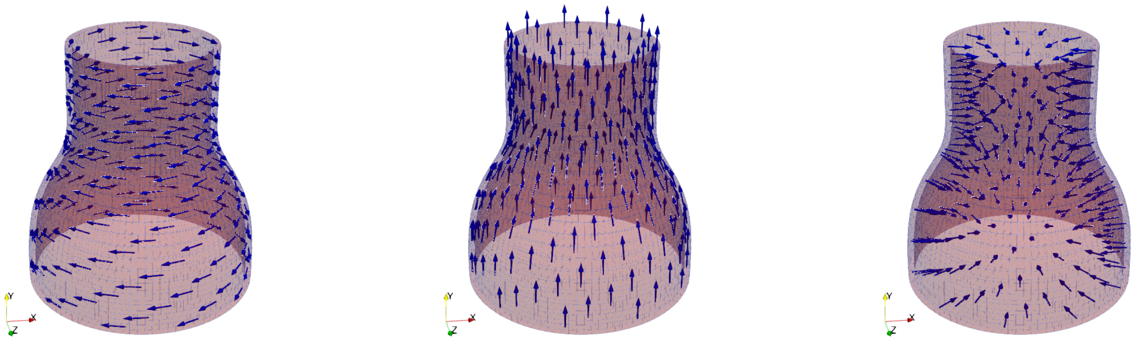

(a) *(b)* *(c)*

Figure 3: (a) Local circumferential, (b) longitudinal and (c) radial reference directions in a generic axisymmetric geometry.

with the axes of an orthotropic material. Specifically, LS-DYNA requires two unit vectors $\boldsymbol{a}$ and $\boldsymbol{d}$ to be provided as input for each element, whereas the unit vectors $\boldsymbol{c} = \boldsymbol{a} \times \boldsymbol{d}$ and $\boldsymbol{b} = \boldsymbol{c} \times \boldsymbol{a}$ are calculated internally, see Figure 4. In the implementation proposed, vector $\boldsymbol{a} \equiv \boldsymbol{E}_1$ defines the local reference circumferential direction and $\mathbf{d} \equiv \boldsymbol{E}_2$ the local reference axial direction. The internally calculated vector $\boldsymbol{c}$ identifies the local reference radial direction. Since $\boldsymbol{a} \perp \boldsymbol{d}$, we clearly have $\boldsymbol{b} \equiv \boldsymbol{d}$.

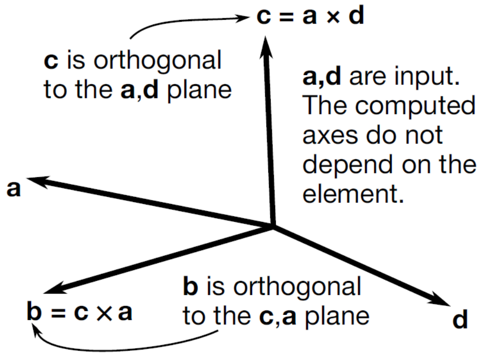

Figure 4: Definition of the LCS if AOPT=2.0 is specified for each element, with $\boldsymbol{b} \equiv \boldsymbol{d}$. Reproduced from LS-DYNA User Manual [3].

Verification

To illustrate the constitutive behaviour described by the model, we have selected three boundary value problems, which can be solved explicitly in the case of perfect incompressibility by considering the plane stress assumption. The selected examples serve as verification of the user-defined material model in ANSYS Mechanical APDL and as representative examples of the LS-DYNA implementation.

Benchmark problems

In order to derive an analytical expression of the stress tensor, let us consider the incompressible strain-energy function (8) combined with expressions (10)-(11). Let us consider two fibre families symmetrically disposed in the circumferential-axial plane $\boldsymbol{E}_1, \boldsymbol{E}_2$, each making an angle $\pm\alpha$ with respect to the circumferential direction. Then, the in-plane fibre unit vectors $\boldsymbol{M}_4$ and $\boldsymbol{M}_6$ are

$$\boldsymbol{M}_4 = \cos\alpha\boldsymbol{E}_1 + \sin\alpha\boldsymbol{E}_2, \quad \boldsymbol{M}_6 = \cos\alpha\boldsymbol{E}_1 - \sin\alpha\boldsymbol{E}_2, \tag{33}$$

and the out-of-plane unit vector is $\boldsymbol{M}_\mathrm{n} = \boldsymbol{E}_3$.
The Cauchy stress tensor is computed according to [12]

$$\boldsymbol{\sigma} = \mu\mathbf{b} + 2\sum_{i=4,6}\psi_i\mathbf{h}_i - p, \tag{34}$$

where p is a Lagrange multiplier determined by imposing the plane stress condition $\sigma_{33} = 0$.
The structure tensor in the current configuration $\mathbf{h}_i$, as introduced in (16), can be reformulated as

$$\mathbf{h}_i = A\mathbf{b} + B(\boldsymbol{m}_i \otimes \boldsymbol{m}_i) + (1 - 3A - B)(\boldsymbol{m}_\mathrm{n} \otimes \boldsymbol{m}_\mathrm{n}), \quad i = 4, 6\,, \tag{35}$$

where $m_i = \mathbf{F}\cdot\boldsymbol{M}_i$ represents the in-plane fibre orientation in the current configuration and $m_\mathrm{n} = \mathbf{F}\cdot\boldsymbol{M}_\mathrm{n}$. For the verification, the analytical solution is computed in MATLAB and compared with the numerical results obtained from the finite element analyses. The geometry consists of a cube with unstructured mesh, 8-node linear elements with full integration, and mixed formulation for material incompressibility in ANSYS Mechanical APDL. The parameters used in the benchmark problems are listed in *Table* 6. Note that these are literature values [10] and thus are not calibrated to the tissues tested in the experiments.

Benchmark I: uniaxial extension

A deformation characterised by a diagonal deformation gradient can be defined in terms of principal stretches as follows

$$x_1 = \lambda_1 X_1, \quad x_2 = \lambda_2 X_2, \quad x_3 = \lambda_3 X_3, \tag{36}$$

and the invariants and pseudo-invariants of the left Cauchy-Green strain tensor are given by

$$I_1 = \lambda_1^2 + \lambda_2^2 + \lambda_3^2, \tag{37}$$

$$I_i = \lambda_1^2\cos^2\alpha + \lambda_2^2\sin^2\alpha, \quad i = 4, 6, \tag{38}$$

$$I_\mathrm{n} = \lambda_3^2. \tag{39}$$

According to (34), the relevant components of the Cauchy stress tensor are [12]

$$\sigma_{11} = \lambda_1^2[\mu + 4\psi_4(A + B\cos^2\alpha)] - p, \tag{40a}$$

$$\sigma_{22} = \lambda_2^2[\mu + 4\psi_4(A + B\sin^2\alpha)] - p, \tag{40b}$$

$$\sigma_{33} = \lambda_3^2[\mu + 4\psi_4(1 - 2A - B)] - p, \tag{40c}$$

which are derived recalling that $\mathbf{h}_4 = \mathbf{h}_6$ and $\psi_4 = \psi_6$.

Material parameter	Value	Unit
Incompressibility parameter d	0.0	1/kPa
Shear modulus μ	10.07	kPa
Strain-stiffening parameter b	1e-6	-
Angle of 1st fibre family (w.r.t. circ. direction) α_4	47.99	deg
In-plane dispersion parameter κ_{ip}	0.116	-
Out-of-plane dispersion parameter κ_{op}	0.493	-
Fibre shear modulus k_1	5.89	kPa
Fibre strain-stiffening parameter k_2	21.62	-
Angle of 2nd fibre family (w.r.t. circ. direction) α_6	-47.99	deg

Table 6: Summary of material parameters employed in the numerical solution of the benchmark problems.

Let us consider a uniaxial deformation along the principal direction $\boldsymbol{E}_1$,

$$x_1 = \lambda X_1, \quad x_2 = \lambda_2 X_2, \quad x_3 = (\lambda \lambda_2)^{-1} X_3, \tag{41}$$

and the corresponding deformation gradient

$$\mathbf{F} = \lambda \boldsymbol{e}_1 \otimes \boldsymbol{E}_1 + \lambda_2 \boldsymbol{e}_2 \otimes \boldsymbol{E}_2 + (\lambda \lambda_2)^{-1} \boldsymbol{e}_3 \otimes \boldsymbol{E}_3. \tag{42}$$

The analytical solution is obtained implicitly from (40), with the condition $\sigma_{22} = \sigma_{33} = 0$ and the incompressibility constraint $\lambda_1 \lambda_2 \lambda_3 = 1$. The comparison with the finite element results is illustrated in *Figure* 5.

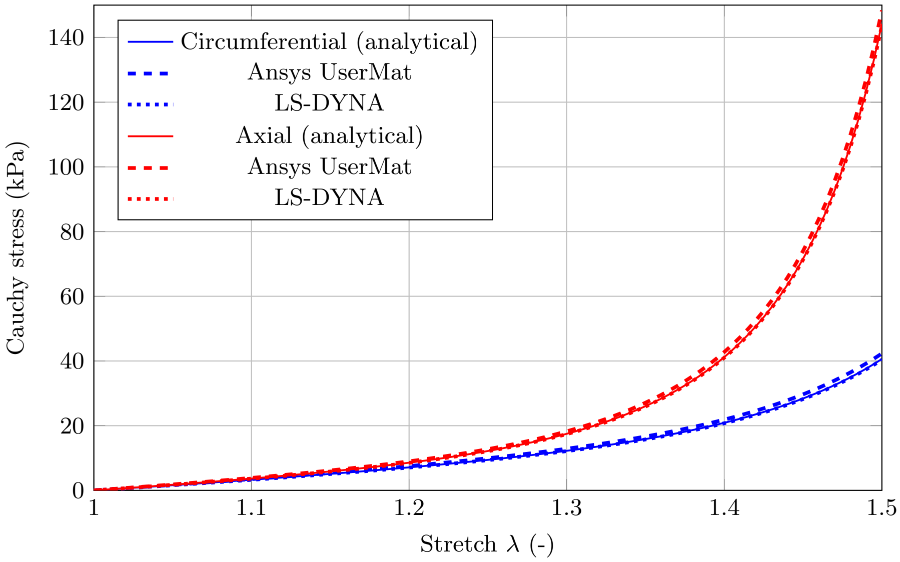

Figure 5: Uniaxial extension. Comparison between analytical solution and numerical results obtained from ANSYS Mechanical APDL and LS-DYNA.

Benchmark II: equibiaxial extension

Let us now consider an equibiaxial deformation in the plane $\boldsymbol{E}_1, \boldsymbol{E}_2$,

$$x_1 = \lambda X_1, \quad x_2 = \lambda X_2, \quad x_3 = \lambda^{-2} X_3, \tag{43}$$

and the corresponding deformation gradient

$$\mathbf{F} = \lambda \boldsymbol{e}_1 \otimes \boldsymbol{E}_1 + \lambda \boldsymbol{e}_2 \otimes \boldsymbol{E}_2 + \lambda^{-2} \boldsymbol{e}_3 \otimes \boldsymbol{E}_3. \tag{44}$$

The components of the Cauchy stress tensor, from (40), are expressed as

$$\sigma_1 = \mu(\lambda^2 - \lambda^{-4}) + 4\psi_4[\lambda^2(A + B\cos^2\alpha) + \lambda^{-4}(2A + B - 1)], \tag{45a}$$

$$\sigma_2 = \mu(\lambda^2 - \lambda^{-4}) + 4\psi_4[\lambda^2(A + B\sin^2\alpha) + \lambda^{-4}(2A + B - 1)], \tag{45b}$$

$$\sigma_3 = 0. \tag{45c}$$

A comparison between analytical solution (45) and numerical results is illustrated in *Figure* 6.

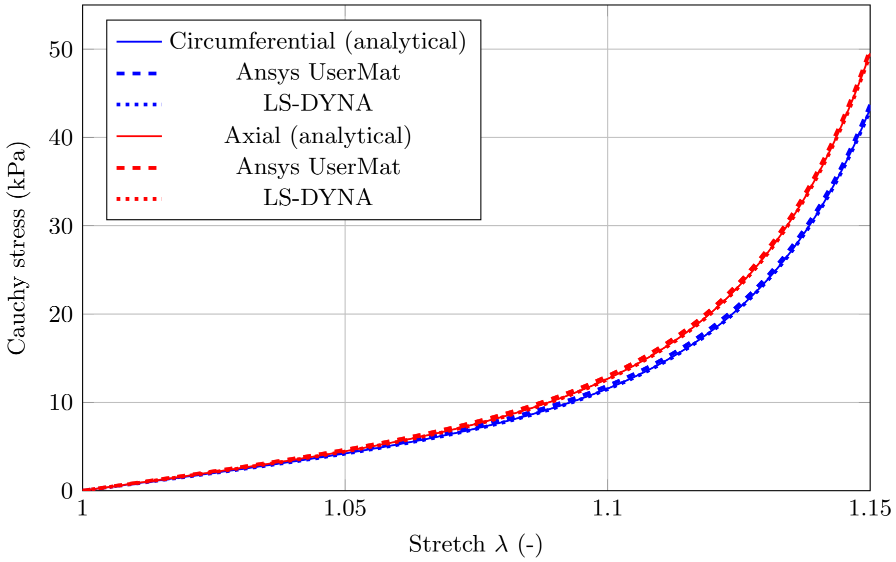

Figure 6: Equibiaxial extension. Comparison between analytical solution and numerical results obtained from ANSYS Mechanical APDL and LS-DYNA.

Benchmark III: simple shear

Finally, let us introduce a simple shear deformation

$$x_1 = X_1 + \gamma X_2, \quad x_2 = X_2, \quad x_3 = X_3, \tag{46}$$

where γ is the amount of shear, and the corresponding deformation gradient

$$\mathbf{F} = \boldsymbol{e}_1 \otimes \boldsymbol{E}_1 + \boldsymbol{e}_2 \otimes \boldsymbol{E}_2 + \boldsymbol{e}_3 \otimes \boldsymbol{E}_3 + \gamma \boldsymbol{e}_1 \otimes \boldsymbol{E}_2. \tag{47}$$

In this case, the invariants and pseudo-invariants of the left Cauchy-Green strain tensor can be expressed in terms of the amount of shear as

$$I_1 = 3 + \gamma^2, \tag{48}$$

$$I_4 = (1 + \gamma^2)\sin^2\alpha + 2\cos\alpha\sin\alpha + \cos^2\alpha, \tag{49}$$

$$I_6 = (1 + \gamma^2)\sin^2\alpha - 2\cos\alpha\sin\alpha + \cos^2\alpha, \tag{50}$$

$$I_\mathrm{n} = 1, \tag{51}$$

Similarly to the previous benchmark problems, the principal Cauchy stress components are obtained from (34), recalling that this time the deformation gradient is not diagonal, therefore $\mathbf{h}_4 \neq \mathbf{h}_6$ and $\psi_4 \neq \psi_6$. The explicit expression of the Lagrange multiplier enforcing the incompressibility constraint is

$$p = \mu + 2(\psi_4 + \psi_6)(1 - 2A - B). \tag{52}$$

Finally, the Cauchy shear stress is calculated from

$$\sigma_{12} = \mu(1 + \gamma^2) + 2 \sum_{i=4,6} \psi_i h_{i\,12} - p, \tag{53}$$

with $h_{i\,12}$ the component of the structure tensor in the current configuration, as defined in (35). A comparison between analytical solution and numerical results is illustrated in *Figure* 7.

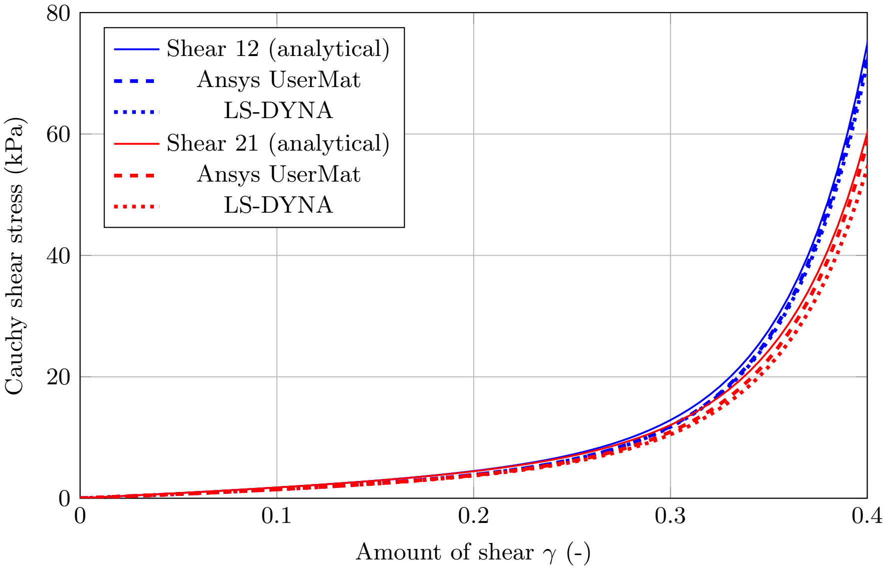

Figure 7: Simple shear. Comparison between analytical solution and numerical results obtained from ANSYS Mechanical APDL and LS-DYNA.

Parameter identification

Similarly to *Deliverable 8.4 - Constitutive vessel model (TUG, M20)*, the parameter identification with the related uncertainty quantification is performed in two steps. First, the constitutive parameters are identified by using representative literature data from the ascending aorta and the pulmonary artery, see *D8.4*. Specifically, experimental results from equibiaxial tensile tests are obtained from the study of Azadani et al. [4] on healthy human tissue, and Matthews et al. [14] on fresh porcine tissue. To decrease the uncertainties related the experimental data coming from different laboratories, we aim to use as less experimental studies as possible. Secondly, after obtaining the full set of experimental results from our laboratory, the constitutive parameters are determined. Experimental results from our laboratory can then also be compared with the available experimental data from literature. In addition, a Bayesian approach, similar to the approach presented in Ranftl et al. [15], is shown that allows to assess the uncertainties in the material parameters. As it was not planned to propagate the uncertainties through from the experiments to the computational models in the following WPs, this approach is only exemplified for one representative example.

Literature

In the following, experimental results from equibiaxial extension tests obtained from literature are presented. In particular, we reprinted the results obtained in the study of Azadani et al. [4] and Matthews et al. [14]. Azadani et al. [4] performed equibiaxial extension tests on healthy human tissue, especially on the ascending aorta and the pulmonary artery. Similarly, in the study of Matthews et al. [14], equibiaxial extension test results were conducted on fresh porcine tissue, again on the ascending aorta and the pulmonary artery. For the purpose of this delivery, it is advantageous to use data from only two studies. Unfortunately, the literature does not provide appropriate data from sheep tissue. The data is shown in *D8.4*.

Non-linear least squares method

The constitutive parameters were determined by minimising an objective function via nonlinear least-square analysis, implemented in MATLAB. The objective function is defined as the sum of the squared differences between the analytically predicted Cauchy stress and the experimental measured values over the number of experimental data points, for an equibiaxial deformation. Then, the built-in function *lsqnonlin* was used to solve the described minimisation problem. The fitting procedure was performed about 1 000 times for each data set using different starting points, and the set of parameters with the lowest residual norm was regarded as best fit.

Results

In the following, the results of the parameter identification for the Holzapfel-Gasser-Ogden model are presented, see*Table* 7 and *Figures* 8-9.

	Parameter						
	μ (kPa)	k_1 (kPa)	k_2 (–)	α deg	κ_{ip} (–)	κ_{op} (–)	R^2 (–)
Ascending Aorta							
Human	28.52	151.97	4.36	55.47	0.409	0.297	0.997
Porcine	17.51	11.14	0.00	15.05	0.329	0.490	0.999
Pulmonary artery							
Human	15.36	119.86	30.99	57.21	0.636	0.282	0.994
Porcine	1.62	8.04	0.13	22.50	0.388	0.500	0.999

Table 7: Parameter identification of the Holzapfel-Gasser-Ogden model for ascending aorta and pulmonary artery (human and porcine tissue).

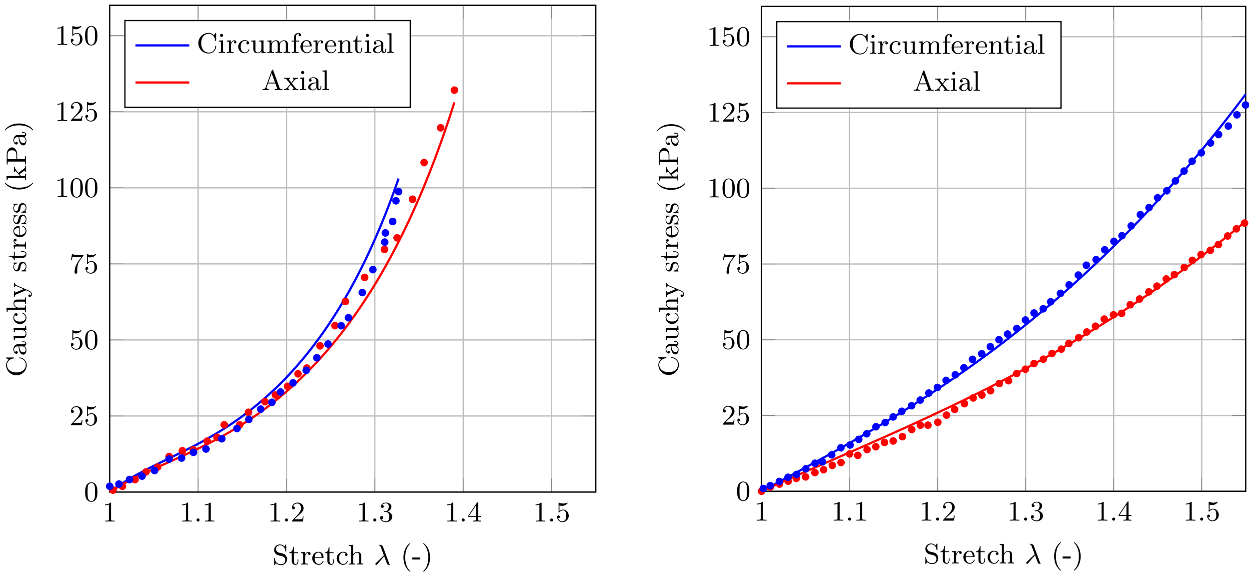

(a) *(b)*

Figure 8: Parameter identification of Holzapfel-Gasser-Ogden model for human (a) and porcine (b) ascending aorta. The plots show the comparison between equibiaxial tensile experiment (dots) and results from parameter identification (line).

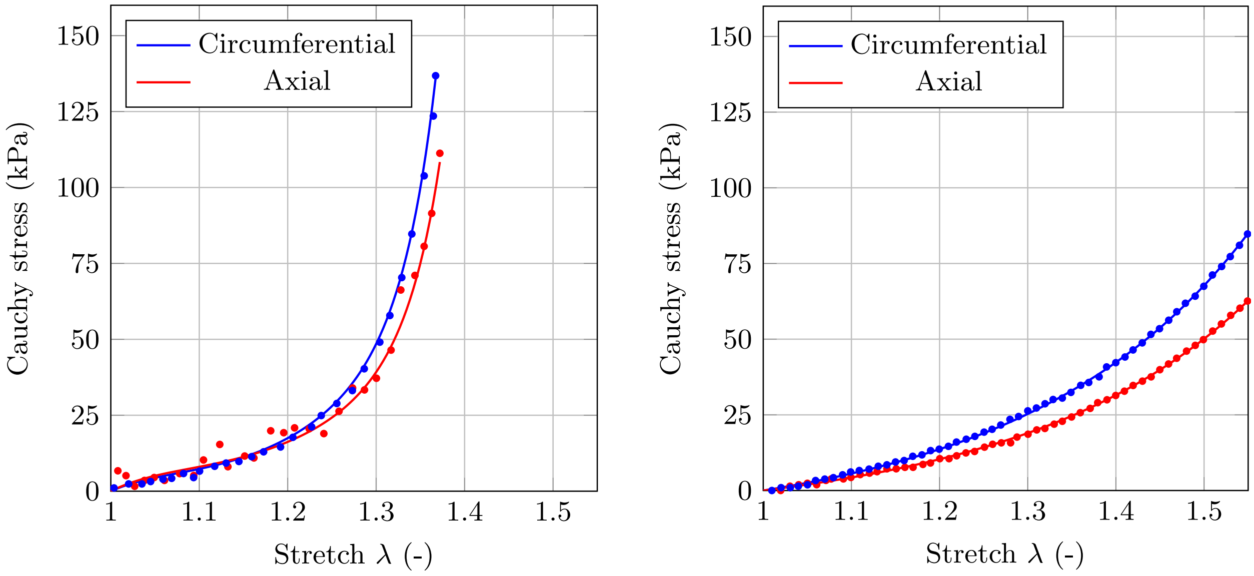

(a) *(b)*

Figure 9: Parameter identification of Holzapfel-Gasser-Ogden model for human (a) and porcine (b) pulmonary artery. The plots show the comparison between equibiaxial tensile experiment (dots) and results from parameter identification (line).

Laboratory (Institute of Biomechanics, TUG)

In this section we present the results of parameter identification based on the experimental results from our laboratory on porcine, sheep and human samples. Missing information in the tables indicates that the specific tissue sample failed prematurely or data was not suitable for post-processing.

Non-linear least squares method

Similar to the previous section, the constitutive parameters were determined through non-linear least-squares analysis to minimise an objective function. The objective function is defined as the sum of squared differences between the analytically predicted Cauchy stress and the measured experimental values, divided by the number of experimental data points. The experimental data were described in *D8.4*. To obtain the analytical solution of the Cauchy stress for the equibiaxial extension test, we utilised the previously proposed strain-energy functions in MATLAB. We then utilised the built-in function *lsqnonlin* to solve the minimisation problem as described.

Results

In the following, the results of the parameter identification with the non-linear least squares methods are presented. The material parameters determined for the Holzapfel-Gasser-Ogden model are reported in textitTables 8-10. The stress versus stretch curves from the experiments and those predicted by the model fitting are shown in *Figures* 17-28 in the Appendix. Equibiaxial extension results (strain ratio 1:1) were fitted until failure.
The Holzapfel-Gasser-Ogden model is able to represent the exponential material behaviour well and it is able to account for anisotropy, that is, it can capture the different behaviour in the circumferential and axial direction. In general, care should be taken when evaluating the fitting performance based on the R^2 value, since this is a poor indicator for nonlinear regression analysis.

Ascending Aorta

Sample	1	2	3	4	5	6	7	8	9	10	11
μ (kPa)	20.54	30.90	31.14	54.84	48.91	49.96	25.94	39.47	65.53	65.36	24.30
k_1 (kPa)	12.46	22.77	21.19	8.02	12.46	17.90	14.72	21.27	0.29	0.72	13.11
k_2 (–)	0.10	1.00	0.90	0.00	0.83	2.50	0.36	1.80	0.00	18.51	0.39
α (deg)	27.58	34.80	40.16	0.00	42.28	28.93	38.44	47.04	0.00	59.65	23.48
κ_{ip} (–)	0.29	0.33	0.39	0.00	0.24	0.25	0.28	0.31	0.00	0.28	0.24
κ_{op} (–)	0.50	0.35	0.40	0.50	0.50	0.50	0.47	0.33	0.50	0.48	0.50
R^2 (–)	0.99	0.99	0.99	0.98	0.99	0.99	0.99	0.99	0.96	0.99	0.99

Main Pulmonary Artery

Sample	1	2	3	4	5	6	7	8	9	10	11
μ (kPa)	9.13	6.36	14.23	9.62	10.06		9.23	8.59	8.97	9.51	7.54
k_1 (kPa)	3.85	4.98	0.56	2.68	4.01		4.23	4.59	1.20	7.07	3.21
k_2 (–)	2.46	1.52	4.22	2.63	2.20		1.22	1.67	1.34	0.85	1.37
α (deg)	25.18	1.52	1.00	1.77	0.12		1.12	3.74	0.23	7.12	1.33
κ_{ip} (–)	0.47	0.39	0.50	0.39	0.45		0.43	0.31	0.46	0.42	0.42
κ_{op} (–)	0.48	0.34	0.33	0.33	0.33		0.33	0.34	0.33	0.33	0.33
R^2 (–)	0.99	0.99	0.90	0.99	0.99		0.99	0.99	0.99	0.99	0.99

Left Pulmonary Artery

Sample	1	2	3	4	5	6	7	8	9	10	11
μ (kPa)	12.04	10.45	11.52	6.73	10.84		8.65	10.66	9.49	13.07	11.91
k_1 (kPa)	43.11	26.05	28.45	28.96	24.66		19.96	19.95	8.81	51.07	15.45
k_2 (–)	8.33	2.92	3.64	5.46	8.14		6.26	3.18	1.21	4.69	1.63
α (deg)	10.48	4.25	5.78	36.34	27.49		7.05	1.00	2.55	10.27	1.36
κ_{ip} (–)	0.38	0.33	0.37	0.42	0.47		0.36	0.50	0.41	0.37	0.42
κ_{op} (–)	0.33	0.35	0.33	0.33	0.34		0.33	0.38	0.33	0.33	0.33
R^2 (–)	0.99	0.99	0.99	0.99	0.99		0.99	0.9	0.99	1.00	1.00

Continued on the next page

Right Pulmonary Artery											
Sample	1	2	3	4	5	6	7	8	9	10	11
μ (kPa)	11.84	10.45	4.36	5.72	3.25	6.55	13.25		8.40	5.50	12.46
k_1 (kPa)	22.71	9.12	17.18	18.27	10.55	15.67	26.63		52.68	9.03	57.60
k_2 (–)	4.40	1.93	2.67	4.55	0.64	1.75	3.10		8.35	0.63	8.88
α (deg)	5.01	1.56	1.00	8.56	28.50	1.22	13.60		9.10	1.31	9.99
κ_{ip} (–)	0.33	0.41	0.50	0.46	0.37	0.31	0.47		0.36	0.43	0.37
κ_{op} (–)	0.39	0.37	0.42	0.35	0.50	0.34	0.33		0.33	0.38	0.33
R^2 (–)	1.00	0.99	0.99	0.99	0.99	0.99	1.00		1.00	0.99	0.99

Table 8: Parameter identification of the Holzapfel-Gasser-Ogden model for porcine ascending aorta and pulmonary artery.

Ascending Aorta									
Sample	1	2	3	4	5	6	7	8	9
μ (kPa)	0.16	6.04	53.35	6.14	30.80	9.81	44.52	33.21	17.11
k_1 (kPa)	11.86	10.44	0.01	7.71	2.96	17.50	1.61	6.89	7.50
k_2 (–)	0.00	0.28	50.00	0.38	0.87	0.06	10.64	4.09	0.11
α (deg)	6.61	2.84	22.89	3.97	0.05	3.69	84.42	0.88	1.02
κ_{ip} (–)	0.46	0.39	0.25	0.42	0.19	0.24	0.30	0.26	0.41
κ_{op} (–)	0.45	0.50	0.45	0.50	0.50	0.50	0.41	0.43	0.50
R^2 (–)	0.99	0.99	0.97	0.99	0.99	0.99	0.94	0.95	0.99
Main Pulmonary Artery									
Sample	1	2	3	4	5	6	7	8	9
μ (kPa)	8.13	2.85	7.49	5.98	2.52	2.35			7.60
k_1 (kPa)	6.96	4.51	2.55	3.01	3.97	3.80			4.29
k_2 (–)	5.87	0.23	9.97	1.78	0.41	0.36			0.74
α (deg)	1.00	0.77	0.94	2.67	1.00	26.92			2.20
κ_{ip} (–)	0.50	0.38	0.43	0.48	0.50	0.44			0.39
κ_{op} (–)	0.33	0.50	0.35	0.50	0.38	0.34			0.40
R^2 (–)	0.97	0.99	0.9	1	0.98	0.99			0.99
Left Pulmonary Artery									
Sample	1	2	3	4	5	6	7	8	9
μ (kPa)	8.37	10.36	3.27	4.42	4.47				
k_1 (kPa)	6.72	0.07	6.77	1.73	2.53				
k_2 (–)	1.84	11.05	0.94	0.62	1.93				
α (deg)	1.00	1.00	1.60	0.86	1.00				
κ_{ip} (–)	0.50	0.50	0.48	0.41	0.50				
κ_{op} (–)	0.33	0.33	0.39	0.40	0.33				
R^2 (–)	0.99	0.98	0.99	0.99	0.99				

Continued on the next page

Right Pulmonary Artery									
Sample	1	2	3	4	5	6	7	8	9
μ (kPa)		4.35	5.90	4.64	0.92				
k_1 (kPa)		4.36	3.07	29.21	4.09				
k_2 (–)		2.45	1.10	4.00	0.00				
α (deg)		9.73	46.65	21.25	42.63				
κ_{ip} (–)		0.42	0.47	0.23	0.12				
κ_{op} (–)		0.33	0.33	0.33	0.44				
R^2 (–)		0.99	0.99	0.99	0.99				

Table 9: Parameter identification of the Holzapfel-Gasser-Ogden model for sheep ascending aorta and pulmonary artery.

Ascending Aorta					
Sample	1	2	3	4	5
μ (kPa)		10.49	12.44		
k_1 (kPa)		23.07	23.77		
k_2 (–)		18.66	36.13		
α (deg)		8.56	8.60		
κ_{ip} (–)		0.47	0.41		
κ_{op} (–)		0.33	0.33		
R^2 (–)		0.99	0.99		
Main Pulmonary Artery					
Sample	1	2	3	4	5
μ (kPa)	2.64	9.42	8.42	7.93	8.83
k_1 (kPa)	1.28	3.84	4.30	11.48	0.15
k_2 (–)	10.68	16.12	25.62	15.19	21.97
α (deg)	61.12	1.00	6.93	14.10	89.99
κ_{ip} (–)	0.35	0.50	0.37	0.32	0.35
κ_{op} (–)	0.50	0.33	0.33	0.34	0.47
R^2 (–)	0.99	0.99	0.99	0.90	0.99
Left Pulmonary Artery					
Sample	1	2	3	4	5
μ (kPa)	8.05		9.94	9.19	7.93
k_1 (kPa)	3.31		0.05	4.86	0.56
k_2 (–)	17.72		43.96	20.34	24.06
α (deg)	78.83		61.66	0.79	61.90
κ_{ip} (–)	0.45		0.33	0.43	0.30
κ_{op} (–)	0.50		0.45	0.33	0.50
R^2 (–)	0.99		0.99	0.99	0.99

Continued on the next page

Right Pulmonary Artery					
Sample	1	2	3	4	5
μ (kPa)	5.12	12.01	6.34	4.38	5.27
k_1 (kPa)	1.19	0.05	18.12	14.78	2.86
k_2 (–)	44.33	16.76	22.40	22.12	50.00
α (deg)	3.61	89.91	72.33	37.13	5.41
κ_{ip} (–)	0.43	0.34	0.45	0.47	0.44
κ_{op} (–)	0.50	0.47	0.36	0.37	0.50
R^2 (–)	0.99	0.99	0.99	0.99	0.99

Table 10: Parameter identification of the Holzapfel-Gasser-Ogden model for human ascending aorta and pulmonary artery.

Bayesian framework

To perform a parameter estimation a Bayesian framework is implemented. A Bayesian framework is a method of statistical interference applying Bayes' theorem to obtain the probability of a certain parameter set. Bayes' theorem for the specific application considered here can be formulated as

$$\rho(\theta \mid \mathrm{P}, \mathrm{F}, \mathcal{H}) \propto \rho(\mathrm{P} \mid \theta, \mathrm{F}, \mathcal{H})\rho(\theta \mid \mathrm{F}, \mathcal{H}). \tag{54}$$

where $\rho(\theta \mid \mathrm{P}, \mathrm{F}, \mathcal{H})$ stands for the posterior probability, which is the probability of a certain θ given P, F and $\mathcal{H}$. Here, P denotes the stress component, F denotes the deformation, and $\mathcal{H}$ denotes the constitutive material model. The posterior probability can be obtained using (54). Here, $\rho(\mathrm{P} \mid \theta, \mathrm{F}, \mathcal{H})$ stands for the probability of observing P given θ, F and $\mathcal{H}$, this is also called the likelihood. Finally, $\rho(\theta \mid \mathrm{F}, \mathcal{H})$ represents the prior probability and is the estimate of the probability of the hypothesis θ given a F and $\mathcal{H}$ before the stress data P is observed. in this case, Jeffery's prior is used, making the posterior invariant under reparametrisation. So, given a $\mathcal{H}$ with θ and F a prediction of the theoretical response P is obtained, around which the experimental stress measurements are assumed to be normally distributed with some unknown variance.

To obtain a set of parameter sets a Metropolis-Hastings algorithm was employed, which is a Markov chain Monte Carlo method. The Metropolis-Hastings algorithm is utilised to obtain a sequence of samples from a probability distribution. In this case, through the Bayesian framework, a log-posterior is used, which represents the logarithm of the posterior probability. The Metropolis-Hastings algorithm is generally implemented for sampling from a multi-dimensional distribution, in this case, six dimensions are used. At first, the Metropolis-Hastings algorithm needs an initial parameter set θ_0, as a starting point. Secondly, starting at this initial point, the algorithm takes candidate samples, which are produced iteratively, and accepts or rejects these candidate samples with some probability. If a candidate sample is accepted, the candidate sample is added to the Markov chain and the algorithm bases the next candidate set on the current candidate set. If the candidate sample gets rejected, it is not added to the Markov chain and the current parameter set gets reused for the next iteration. Finally, the Metropolis-Hastings algorithm obtains a distribution of the six parameters. This distribution shows that some combinations of the six parameters are more probable than others and will have a higher frequency. The more sample parameter values are produced by the Metropolis-Hastings algorithm the more closely the sample distribution will approximate the desired distribution. The initial parameter set θ_0 needed for the Metropolis-Hastings algorithm can be obtained using a Nelder-Mead optimisation as discussed below.

As an input, the Metropolis-Hastings algorithm needs initial values for the six different parameters. The mode of the function can be used as an initial guess, as a lot happens around this value. To obtain this mode a parameter optimisation is done acquiring a maximum of the log-posterior. This optimisation is performed through the Nelder-Mead method. The Nelder-Mead method searches the function for a minimum value. In this particular case, we are aiming to find the maximum value. Therefore, when using the Nelder-Mead method as an optimisation technique, we need to negate the log-posterior by adding a minus sign, effectively converting it into a minimisation problem. Now the Nelder-mead method can be applied to find the maximum value of the log-posterior in a multidimensional space. The Nelder-Mead method is simplex-based, where a simplex is defined as a convex hull of $n+1$ verticles in n dimensions. In this case, the parameter estimation is done in six dimensions, so a simplex with seven vertices is used. During the Nelder-Mead method, the minus log-posterior is evaluated at the vertices of a simplex, and iteratively the maximum is obtained. The parameter set found at this maximum is implemented as the initial guess for the Metropolis-Hastings algorithm.

As an input for the Bayesian framework, the experimental biaxial data of porcine ascending aorta of 11 samples is utilised. To represent physical stretches in porcine ascending aorta, the experimental results until a biaxial stretch of $\lambda = 1.3$ are taken into account. For the samples that ruptured before a stretch of $\lambda = 1.3$, the results until rupture are used, as it can be seen in Appendix. For the parameter estimation, the experimental data of samples P2 and P8 are excluded. These samples showed unphysical behaviour with stretches below zero, see Appendix. Firstly, the results obtained from the optimisation are shown and afterwards the results obtained from the Metropolis-Hastings algorithm.

Results: optimisation

To obtain the parameter estimation, optimisation is performed using the Nelder-Mead method. Based on this, the parameter set that is most likely is obtained. The following values for the parameters are obtained: $\alpha = 0.287$, $\mu = 19.775$, $k_1 = 34.262$, $k_2 = 4.176 \cdot 10^{-6}$, $\kappa_{\mathrm{ip}} = 0.474$ and $\kappa_{\mathrm{op}} = 0.441$. Using these obtained parameters, the biaxial experiments performed on the porcine ascending aorta samples are simulated using a code written in Julia [5]. For sample P3, the results in *Figure* 10 show the nominal stress P against stretch λ, for (a) the circumferential direction $\boldsymbol{E}_1$ and (b) the longitudinal direction $\boldsymbol{E}_2$. The results of the other samples can be found in Appendix. Looking at all the results, it can be seen that for both directions, the simulations tend to overestimate and underestimate the experimental data half of the time. The obtained parameter modes are utilised as an input for the Metropolis-Hastings algorithm, providing a good starting point.

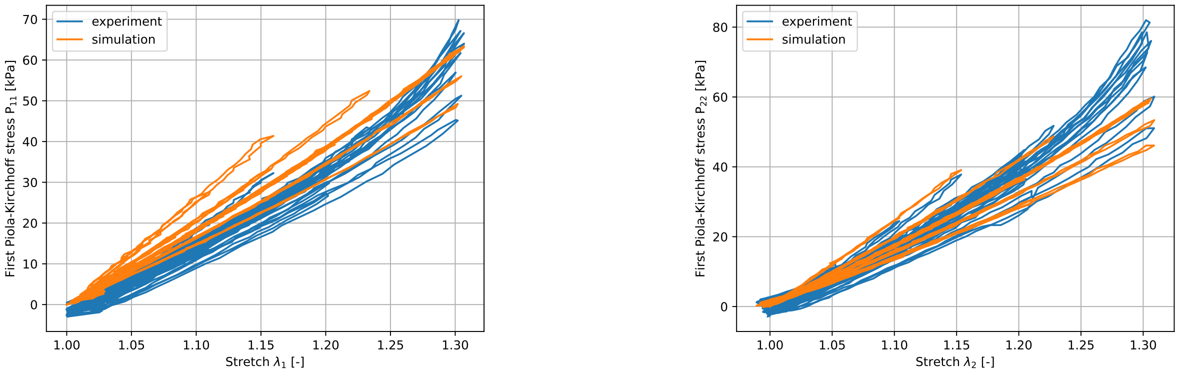

(a) (b)

Figure 10: Results of sample P3 from porcine ascending aorta, for (a) circumferential direction $\boldsymbol{E}_1$ *and (b) longitudinal direction* $\boldsymbol{E}_2$*.. Here 'experiment' refers to the results obtained from the biaxial experiment performed and 'simulation' refers to the results obtained when the parameter mode is used in the simulation with the corresponding stretches.*

Results: Metropolis-Hastings algorithm

A Metropolis-Hastings algorithm is employed to obtain a set of parameter sets that give a good fit to the biaxial experimental data of porcine ascending aorta. Here the optimal parameter set from the Nelder-Mead method is implemented as a good starting point for the algorithm. To obtain a good distribution of the 6 parameters of the Holzapfel-Gasser-Ogden model, 30 000 parameter sets are used to perform the parameter estimation. To visualise the separate parameters marginalised histograms are pictured in *Figure* 11. Here, the distribution obtained for the six different parameters implemented as input for the model proposed by Holzapfel et al. [10] are presented.

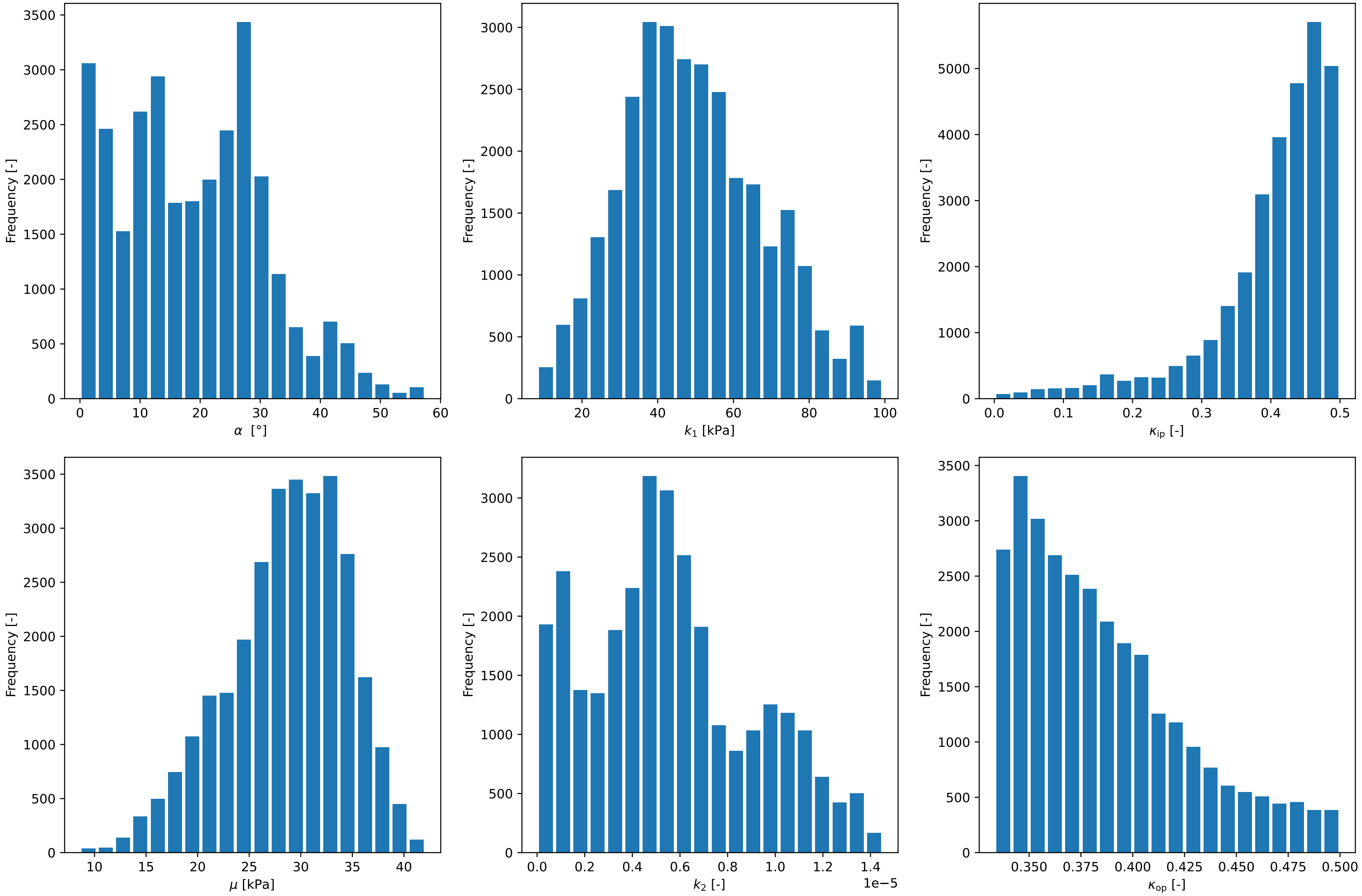

Figure 11: The marginalised distribution of the 6 unknown parameters of the Holzapfel-Gasser-Ogden model obtained during the parameter estimation when using 9 biaxial experiments of porcine ascending aorta.

Figure 11 displays the marginalised distribution of the six parameters, which is a distribution of values of each parameter while ignoring the related parameters in the parameter set. For the fibre angle α, it can be seen that the distribution is uncertain in the range seen in the histogram. Alongside this, it is less probable for the fiber angle α to exceed $40°$, although this observation may also be attributed to the Metropolis-Hastings algorithm not extensively exploring that region due to its initial starting value of $\alpha \approx 16°$. It is important to note that in this study only positive fibre angles are considered. But, as there are two fibre families, the other one has $-\alpha$ as the fibre angle. Secondly, the marginalised distribution of μ, the shear modulus of the non-collagenous ground matrix, is shown. The shear modulus of the non-collagenous ground matrix shows a peek in the histogram and a preference for a value for μ around 30 kPa is found. Next, the marginalised distribution of k_1, the shear modulus of the collagen fibres, is shown in *Figure* 11. Similarly, a peak in the distribution for k_1 is observed, with the highest frequency occurring at $k_1 \approx 40$ kPa.

The dimensionless parameter that controls the strain-stiffening behaviour is represented by k_2. For k_2, it can be seen that the distribution is uncertain in the range of the histogram. In addition, only very small values of k_2 are found in all parameter sets, all being around $1 \cdot 10^{-5}$. For κ_{ip}, representing the in-plane fibre dispersion, a left-skewed distribution can be observed in the visible range, with a maximum occurrence around $\kappa_{\mathrm{ip}} \approx 0.5$. Here the range of κ_{ip} is between 0 and 0.5, which is the range proposed for κ_{ip} [10]. Finally, the marginalised distribution of κ_{op} is visualised in *Figure* 11, representing the out-of-plane fibre dispersion. κ_{op} shows a higher uncertainty in the distribution than κ_{ip} and a right-skewed distribution is observed. The range of κ_{op} is between $1/3$ and 0.5, corresponding to the range of κ_{op} proposed by Holzapfel et al. [10].

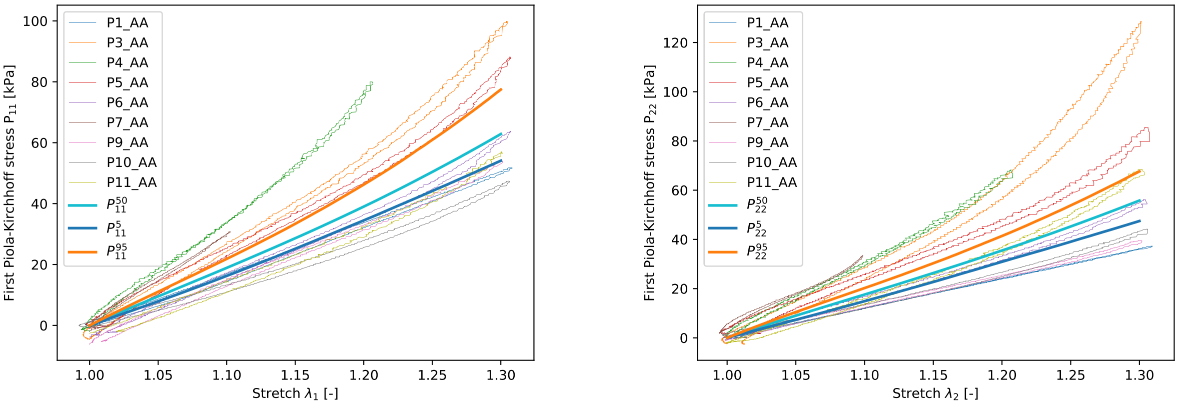

(a) *(b)*

Figure 12: The experimental data of porcine ascending aorta for an equibiaxial stretch of $\lambda = 1.3$. Also, the 50th, 5th, and 95th percentile are shown of the simulation performed with the 30 000 obtained parameter sets. (a) shows the first Piola-Kirchhoff stress P_{11} in the circumferential direction $\boldsymbol{E}_1$. (b) shows the first Piola-Kirchhoff stress P_{22} in the longitudinal direction $\boldsymbol{E}_2$.

For the 30 000 parameter sets that were obtained in the parameter estimation, a simulation is done for an equibiaxial experiment with a maximal stretch of $\lambda = 1.3$. From these simulations, the 50th, 5th, and 95th percentile are shown in *Figure* 12. The area between the 5th and 95th percentile shows the 90% confidence interval of possible average responses. This figure also shows the experimental data of the porcine ascending aorta for an equibiaxial stretch of $\lambda = 1.3$. For experiments P4_AA and P7_AA, which ruptured before a stretch of $\lambda = 1.3$ could be reached, the highest equibiaxial stretch data is used. In *Figure* 12, it can be seen that most of the equibiaxial experimental data does not lie in the 90% interval of possible average responses. Most of the experimental responses have a higher first Piola-Kirchhoff stress than the 90% interval.

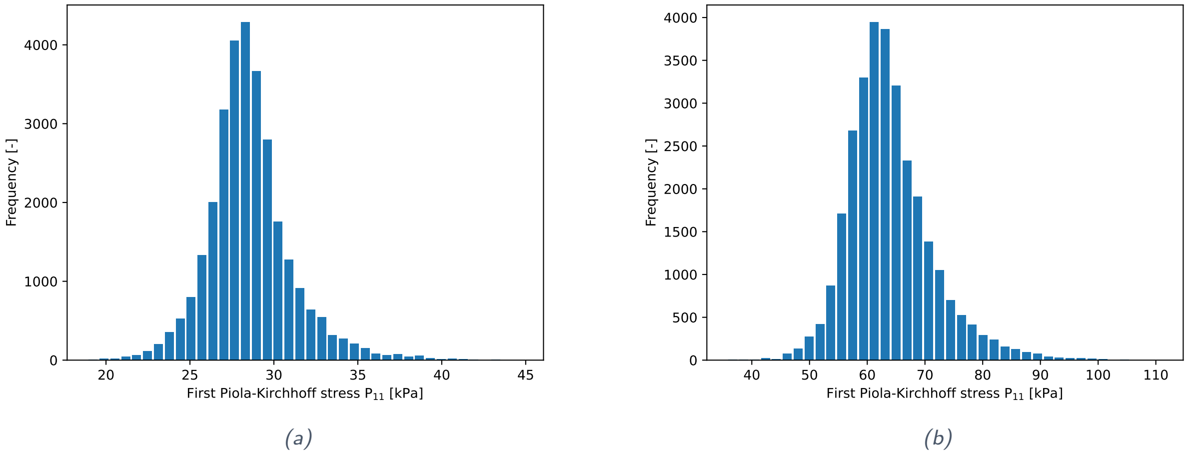

Figure 13: Histogram of the first Piola-Kirchhoff stress P_{11} *from the simulations of the 30 000 obtained parameter sets of the parameter estimation. (a) shows the distribution of* P_{11} *at a stretch of* $\lambda = 1.15$*, halfway through the simulation. (b) shows the distribution of* P_{11} *at a stretch of* $\lambda = 1.3$*, at the end of the simulation.*

In *Figure* 13, the distribution of the first Piola-Kirchhoff stress P_{11} is shown for the simulations of the 30 000 obtained parameter sets of the parameter estimation. The left graph shows the distribution of P_{11} at a stretch of $\lambda = 1.15$, here the distribution appears to be slightly right-skewed. The right graph shows the distribution of P_{11} at a stretch of $\lambda = 1.3$, again, the distribution appears to be slightly right-skewed. This shows overall that the median (50th percentile) lies slightly closer to the 5th percentile than to the 95th percentile in *Figure* 12(a). *Figure* 14 shows the distribution of the first Piola-Kirchhoff stress P_{22} from the simulations of the 30 000 obtained parameter sets of the parameter estimation. The left histogram shows the distribution of the P_{22} at a stretch of $\lambda = 1.15$, based on these results the distribution looks slightly right-skewed. The right histogram shows the distribution of P_{22} at a stretch of $\lambda = 1.3$, again, the distribution appears to be slightly right-skewed. Also for P_{22}, this shows that the median (50th percentile) lies slightly closer to the 5th percentile than to the 95th percentile in *Figure* 12(b).

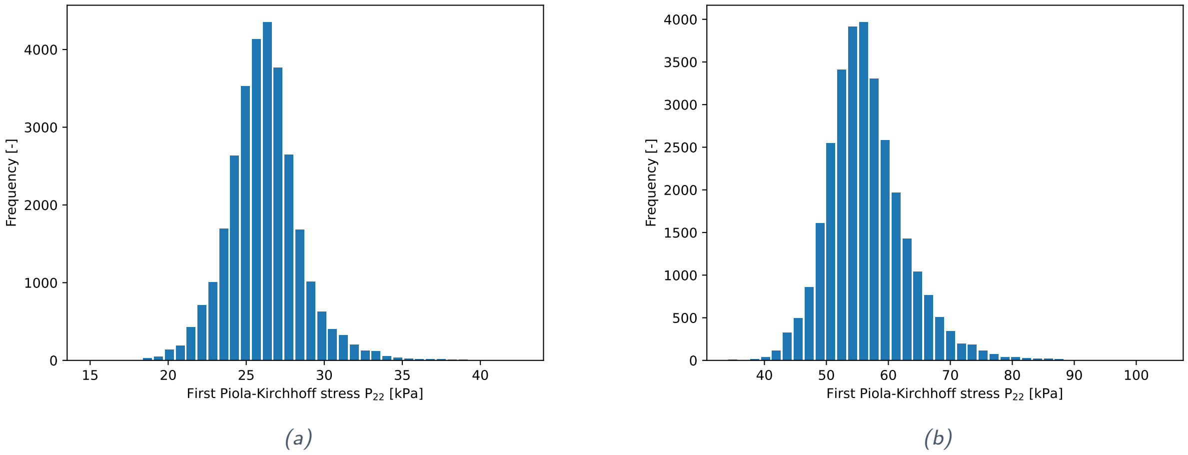

Figure 14: Histogram of the first Piola-Kirchhoff stress P_{22} *from the simulations of the 30 000 obtained parameter sets of the parameter estimation. (a) shows the distribution of* P_{22} *at a stretch of* $\lambda = 1.15$*, halfway through the simulation. (b) shows the distribution of* P_{22} *at a stretch of* $\lambda = 1.3$*, at the end of the simulation.*

Discussion

The vessel constitutive model proposed by Holzapfel et al. [10] was successfully implemented in the commercial finite element software ANSYS Mechanical APDL and LS-DYNA. Since the models are implemented in the in-built model *MAT_295 in LS-DYNA, it was not necessary to verify them. Thus, only the keywords are provided in this deliverable. On the contrary, we implemented the model proposed by Holzapfel et al. [10] into the `UserMat` subroutine of ANSYS Mechanical APDL. Verification activities were therefore required. The comparison between an analytical solution of an equibiaxial extension test, a uniaxial extension test and a simple shear test showed that the results of the numerical solution (ANSYS Mechanical APDL) is in good agreement with the analytical solution. In addition to that, we have developed a framework to implement the material orientation for patient-specific geometries into the two commercial finite element software packages. Initially, the parameters of the Holzapfel-Gasser-Ogden model were derived from existing literature data and subsequently refined using experimental findings from our laboratory for the ascending aorta and the pulmonary artery. We determined the parameters for the main, left, and right pulmonary arteries. Additionally, a Bayesian framework was employed in a representative case study to assess the uncertainty related to these material parameters. While this framework could potentially be applied to the entire data set, we opted to showcase it only for this representative example, as no comprehensive uncertainty quantification was planned for subsequent computational investigations. It is worth noting that this approach is relatively time-consuming in terms of computational modelling.

References

[1] *ANSYS Mechanical APDL – Command Reference (R2021 R1)*. ANSYS Inc., Canonsburg, 2021.

[2] *ANSYS Mechanical APDL – Programmer's Reference (R2021 R1)*. ANSYS Inc., Canonsburg, 2021.

[3] *LS-DYNA Keyword User's Manual Volume II – Material Models (R13)*. Livermore Software Technology Corporation, Livermore, 2022.

[4] A.N. Azadani, S. Chitsaz, P.B. Matthews, N. Jaussaud, J. Leung, A. Wisneski, L. Ge, and E.E. Tseng. Biomechanical comparison of human pulmonary and aortic roots. *Eur J Cardiothorac Surg*, 41(5):1111–6, 2012.

[5] J. Bezanson, A. Edelman, S. Karpinski, and V. B. Shah. Julia: A fresh approach to numerical computing. *SIAM Rev Soc Ind Appl Math*, 59(1):65–98, 2017.

[6] Thomas C Gasser, Raymond W Ogden, and Gerhard A Holzapfel. Hyperelastic modelling of arterial layers with distributed collagen fibre orientations. *Journal of The Royal Society Interface*, 3(6):15–35, 2006.

[7] Osman Gültekin, Hüsnü Dal, and Gerhard A Holzapfel. On the quasi-incompressible finite element analysis of anisotropic hyperelastic materials. *Computational Mechanics*, 63(3):443–453, 2019.

[8] Gerhard A Holzapfel. *Nonlinear Solid Mechanics: A Continuum Approach for Engineering Science*. Wiley, Chichester, 2000.

[9] Gerhard A Holzapfel, Thomas C Gasser, and Raymond W Ogden. A New Constitutive Framework for Arterial Wall Mechanics and a Comparative Study of Material Models. *Journal of Elasticity*, 61(1):1–48, 2000.

[10] Gerhard A Holzapfel, Justyna A Niestrawska, Raymond W Ogden, Andreas J. Reinisch, and Andreas J. Schriefl. Modelling non-symmetric collagen fibre dispersion in arterial walls. *Journal of The Royal Society Interface*, 12(106):20150188, 2015.

[11] Gerhard A Holzapfel and Raymond W Ogden. On the tension–compression switch in soft fibrous solids. *European Journal of Mechanics - A/Solids*, 49:561–569, 2015.

[12] Gerhard A Holzapfel, Raymond W Ogden, and Selda Sherifova. On fibre dispersion modelling of soft biological tissues: a review. *Proceedings of the Royal Society A: Mathematical, Physical and Engineering Sciences*, 475(2224):20180736, 2019.

[13] Cornelius O. Horgan and Michael G Smayda. The importance of the second strain invariant in the constitutive modeling of elastomers and soft biomaterials. *Mechanics of Materials*, 51:43–52, 2012.

[14] P.B. Matthews, A.N. Azadani, C.-S. Jhun, L. Ge, T.S. Guy, J.M. Guccione, and E.E. Tseng. Comparison of porcine pulmonary and aortic root material properties. *Ann Thorac Surg*, 89(6):1981–1988, 2010.

[15] S. Ranftl, T. S. Müller, U. Windberger, G. Brenn, and W. von der Linden. A bayesian approach to blood rheological uncertaintiesin aortic hemodynamics. *Int J Numer Meth Biomed Eng*, page e3576, 2022.

Appendix

Supplementary material - Results of optimisation

Figures 15 and 16 show the results of the porcine ascending aorta samples. Here 'experiment' shows the experimental data from the biaxial experiments and 'simulation' the results obtained from the simulations with the mode parameters.

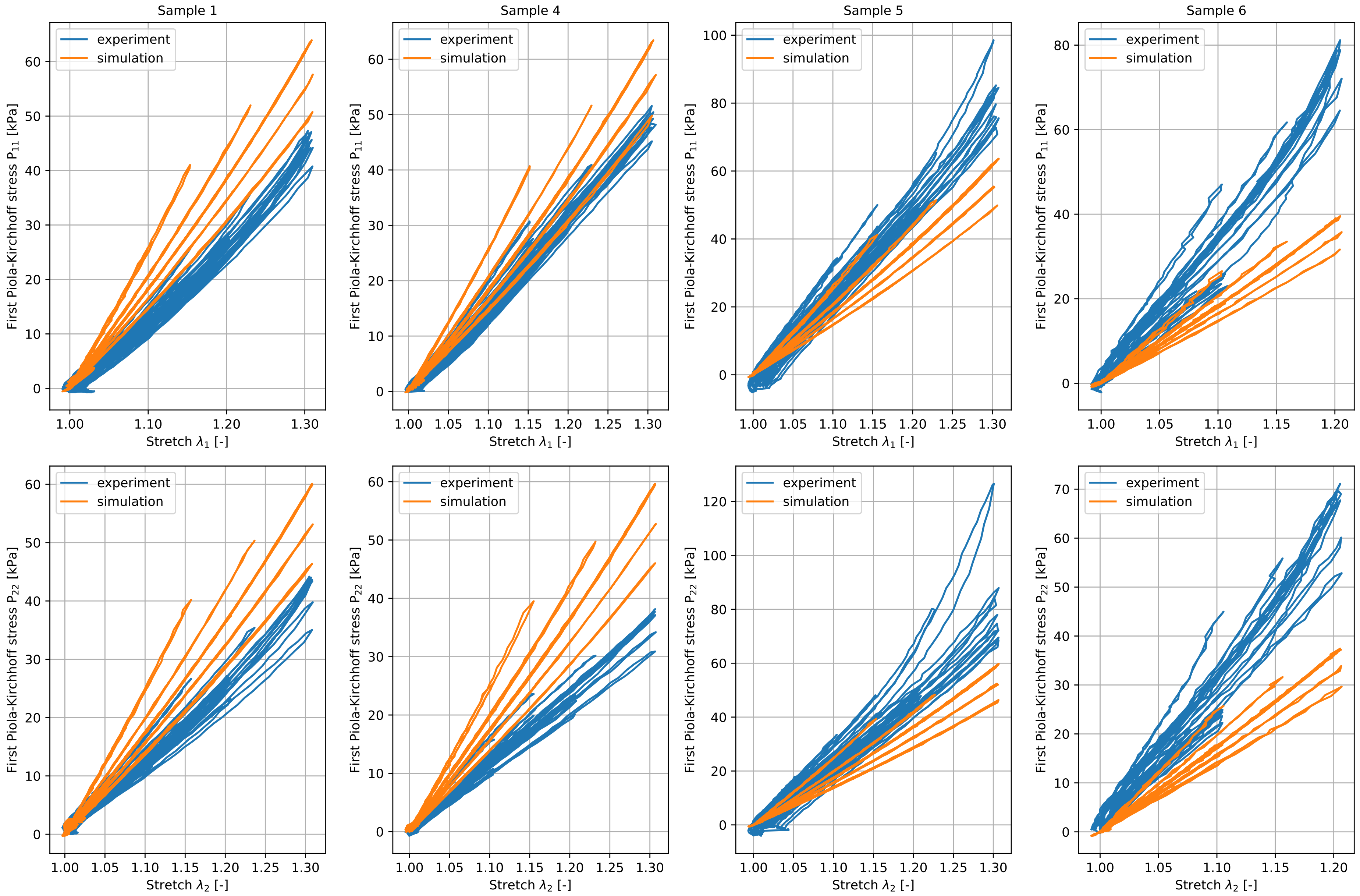

Figure 15: The results of sample 1, 4, 5 and 6 from porcine ascending aorta. Here 'experiment' represents the results from the biaxial experiment performed and 'simulation' represents the results obtained when the parameter mode was used in the simulation with the stretch from the corresponding sample. The top graphs show the extension in the circumferential direction $\boldsymbol{E}_1$ and the bottom graphs show the extension in longitudinal direction $\boldsymbol{E}_2$.

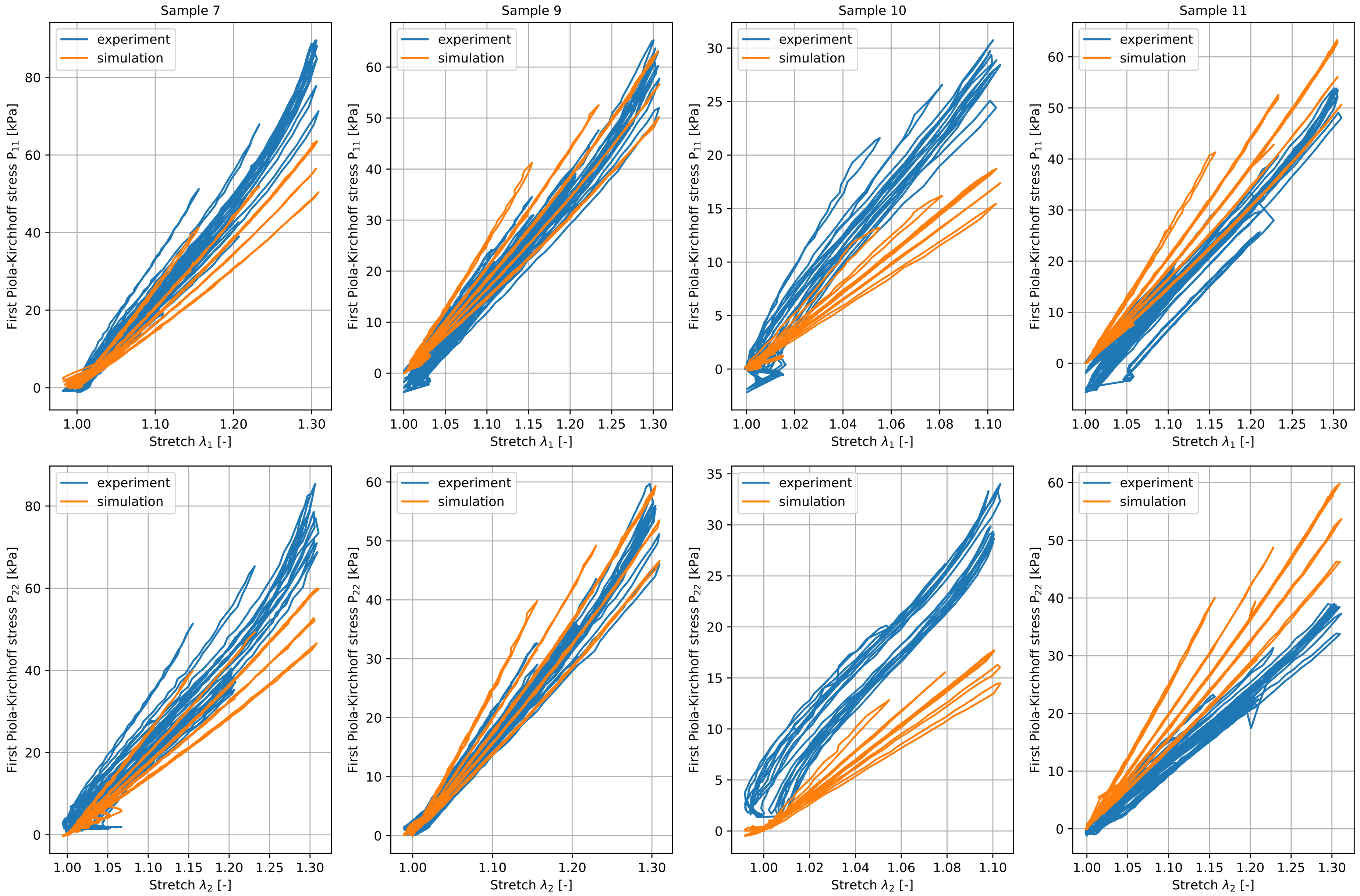

Figure 16: The results of sample 7, 9, 10 and 11 from porcine ascending aorta. Here 'experiment' represents the results from the biaxial experiment performed and 'simulation' represents the results obtained when the parameter mode was used in the simulation with the stretch from the corresponding sample. The top graphs show the extension in the circumferential direction $\boldsymbol{E}_1$ and the bottom graphs show the extension in longitudinal direction $\boldsymbol{E}_2$.

Supplementary material - Parameter identification (porcine)

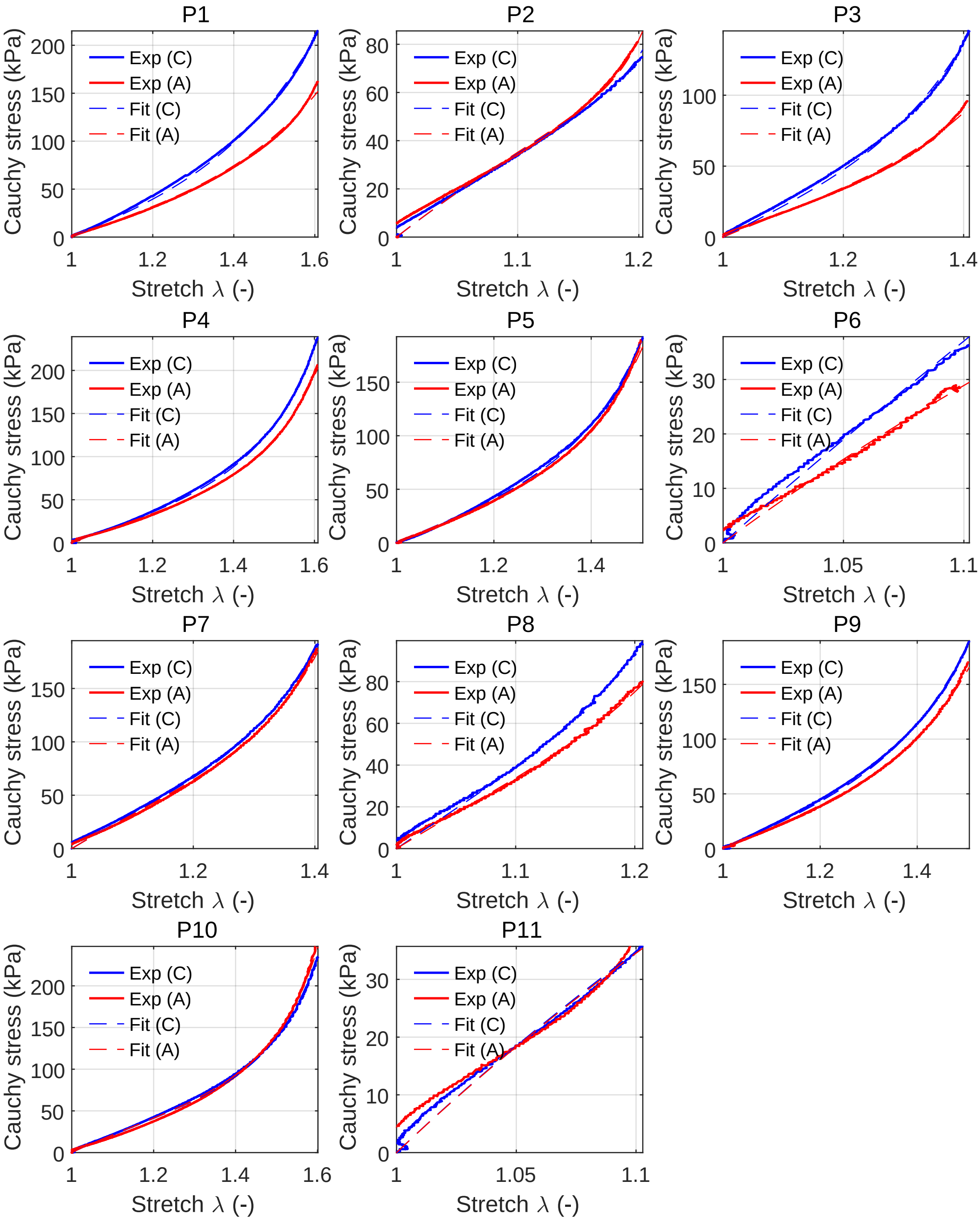

Figure 17: Parameter identification of Holzapfel-Gasser-Ogden model for porcine ascending aorta. The plots show the comparison between experiments and results from parameter identification obtained with MATLAB (C: Circumferential; A: Axial).

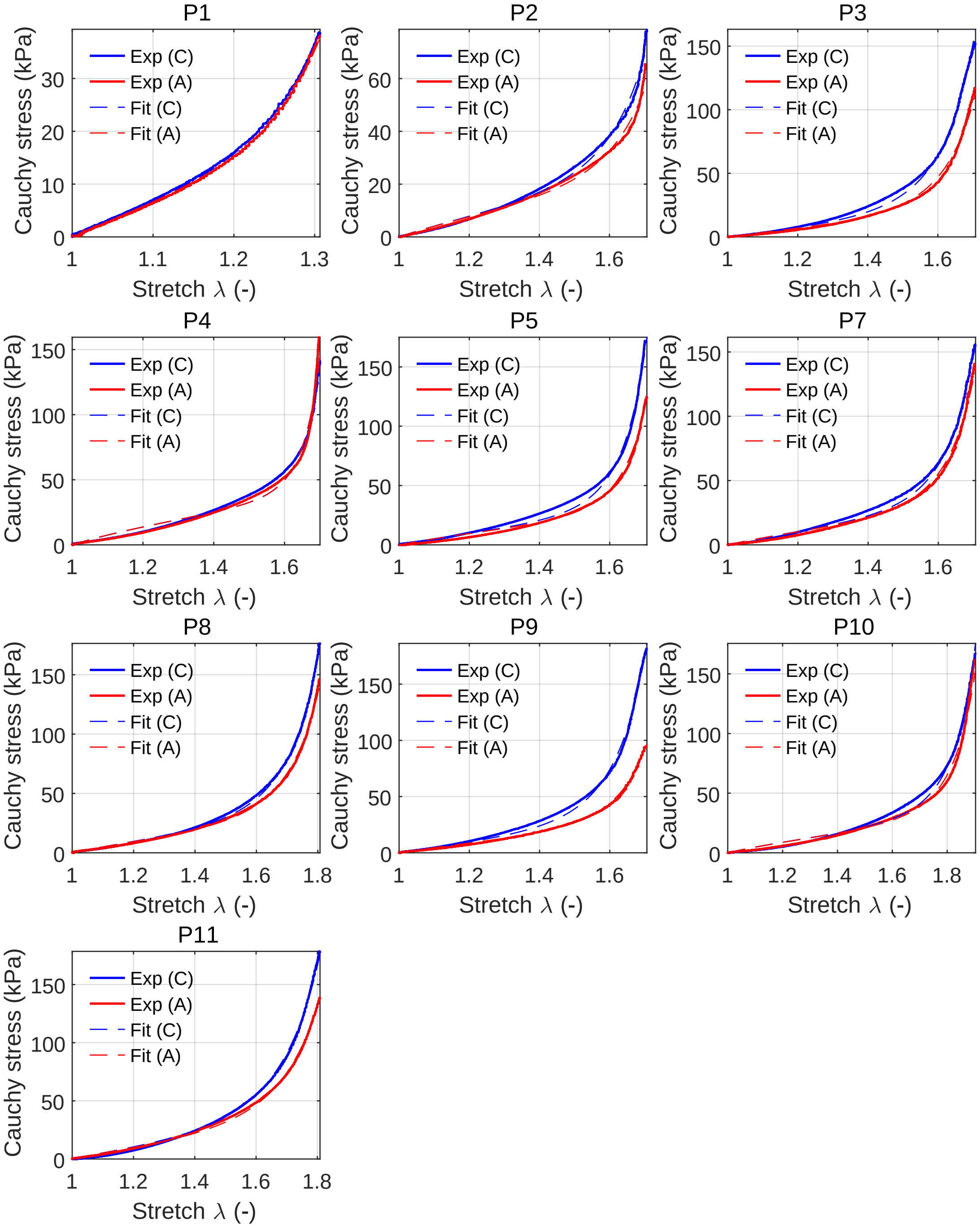

Figure 18: Parameter identification of Holzapfel-Gasser-Ogden model for porcine main pulmonary artery. The plots show the comparison between experiments and results from parameter identification obtained with MATLAB (C: Circumferential; A: Axial).

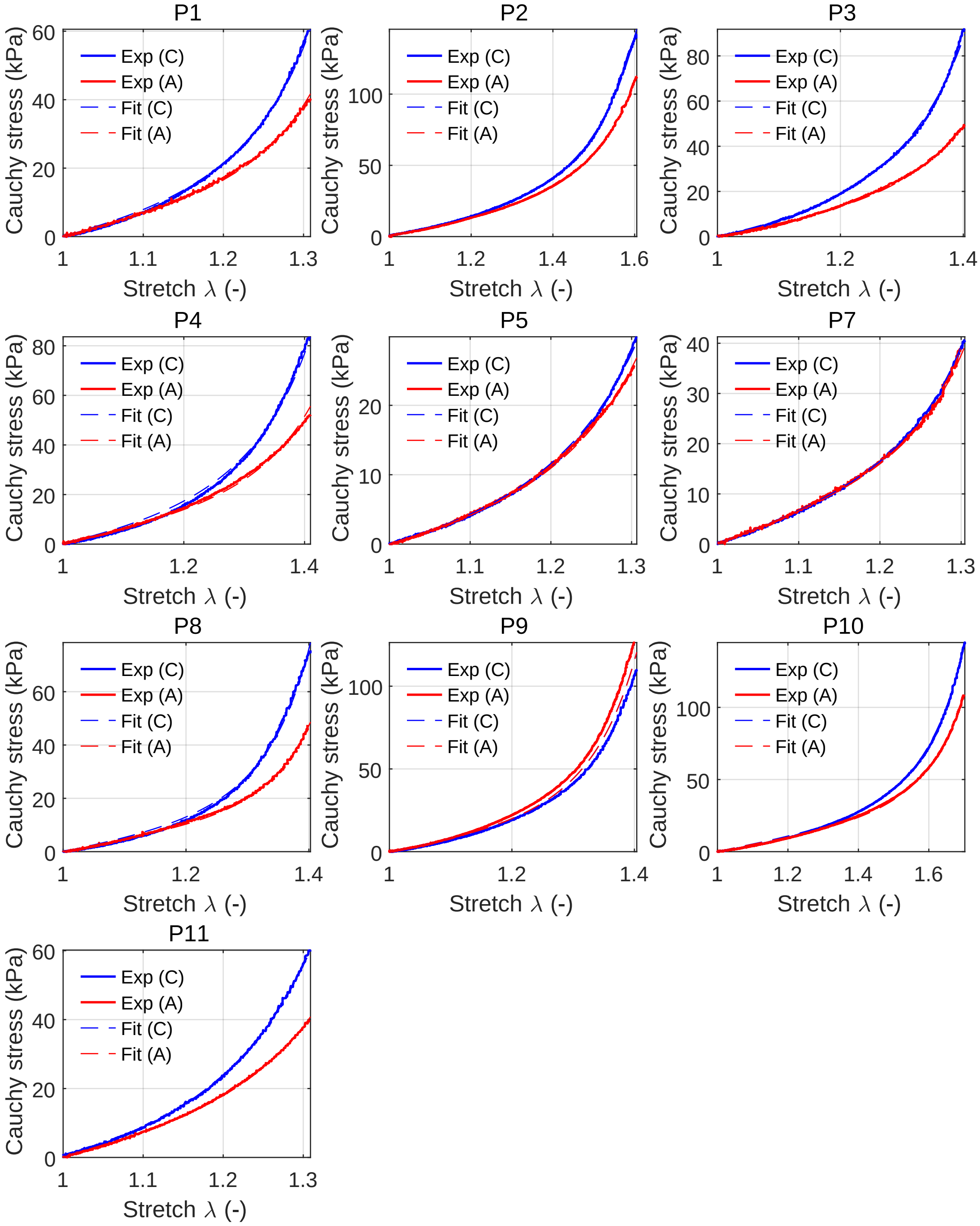

Figure 19: Parameter identification of Holzapfel-Gasser-Ogden model for porcine left pulmonary artery. The plots show the comparison between experiments and results from parameter identification obtained with MATLAB (C: Circumferential; A: Axial).

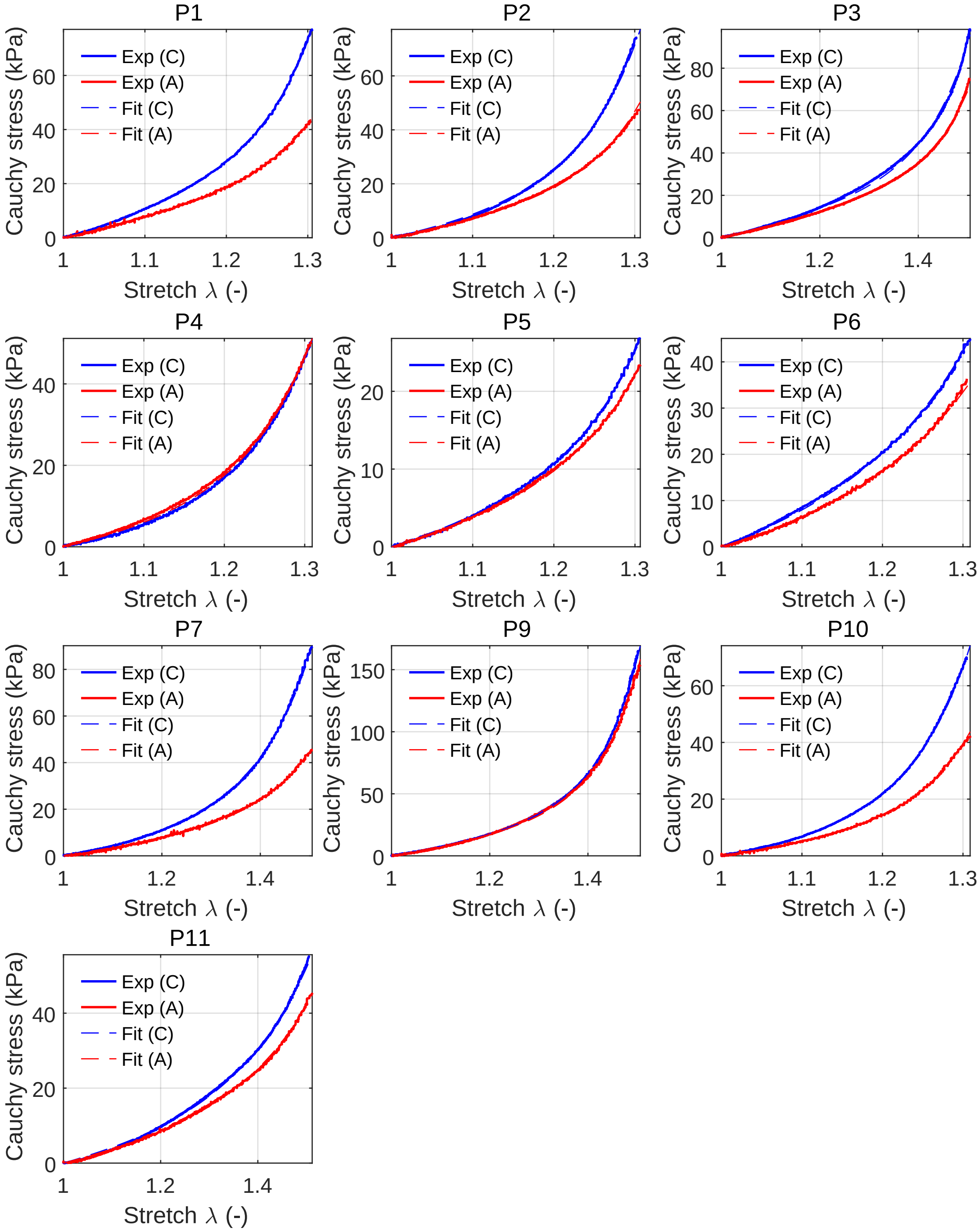

Figure 20: Parameter identification of Holzapfel-Gasser-Ogden model for porcine right pulmonary artery. The plots show the comparison between experiments and results from parameter identification obtained with MATLAB (C: Circumferential; A: Axial).

Supplementary material - Parameter identification (sheep)

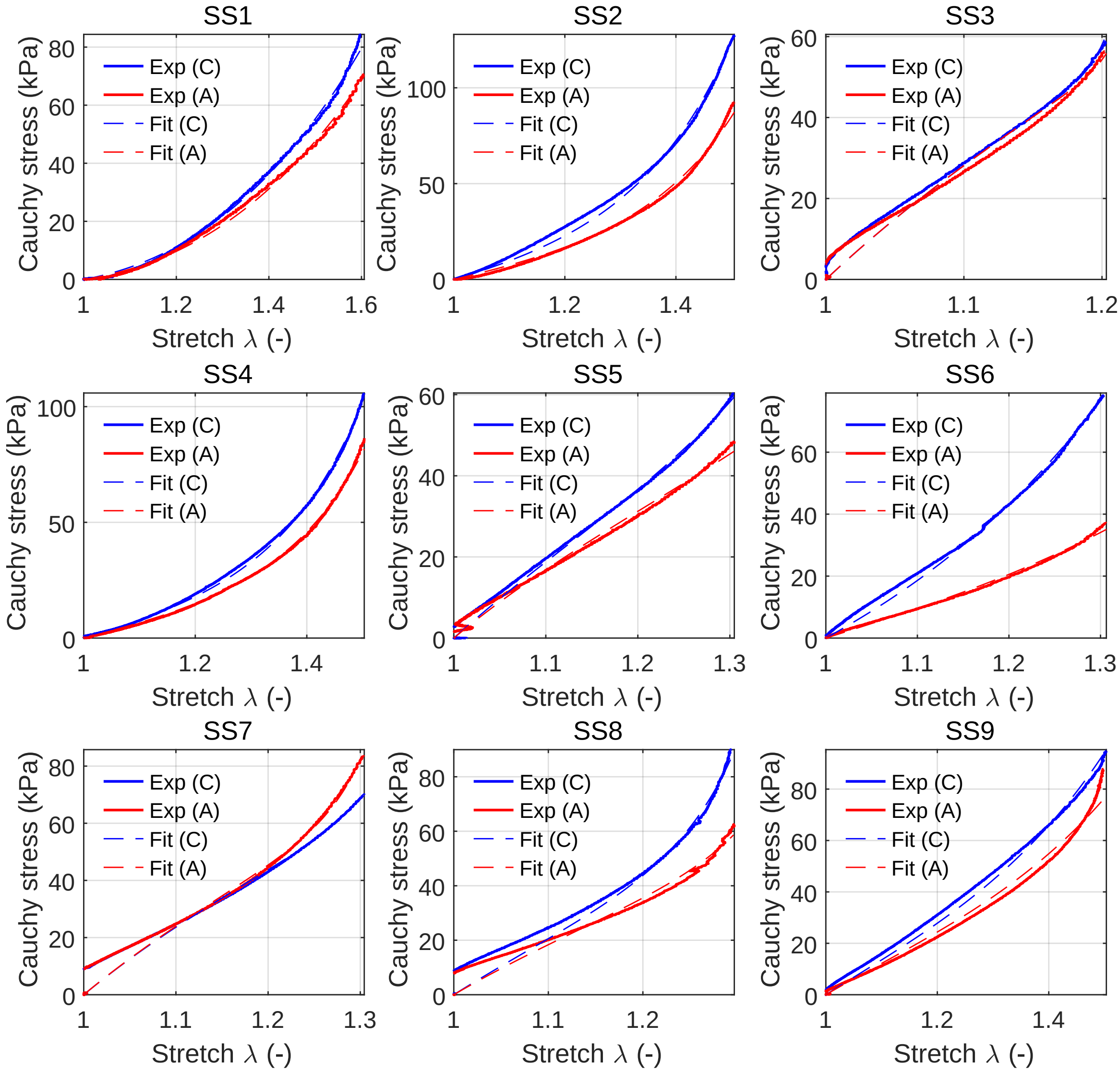
SS1 SS2 SS3 SS4 SS5 SS6 SS7 SS8 SS9

Figure 21: Parameter identification of Holzapfel-Gasser-Ogden model for sheep ascending aorta. The plots show the comparison between experiments and results from parameter identification obtained with MATLAB (C: Circumferential; A: Axial).

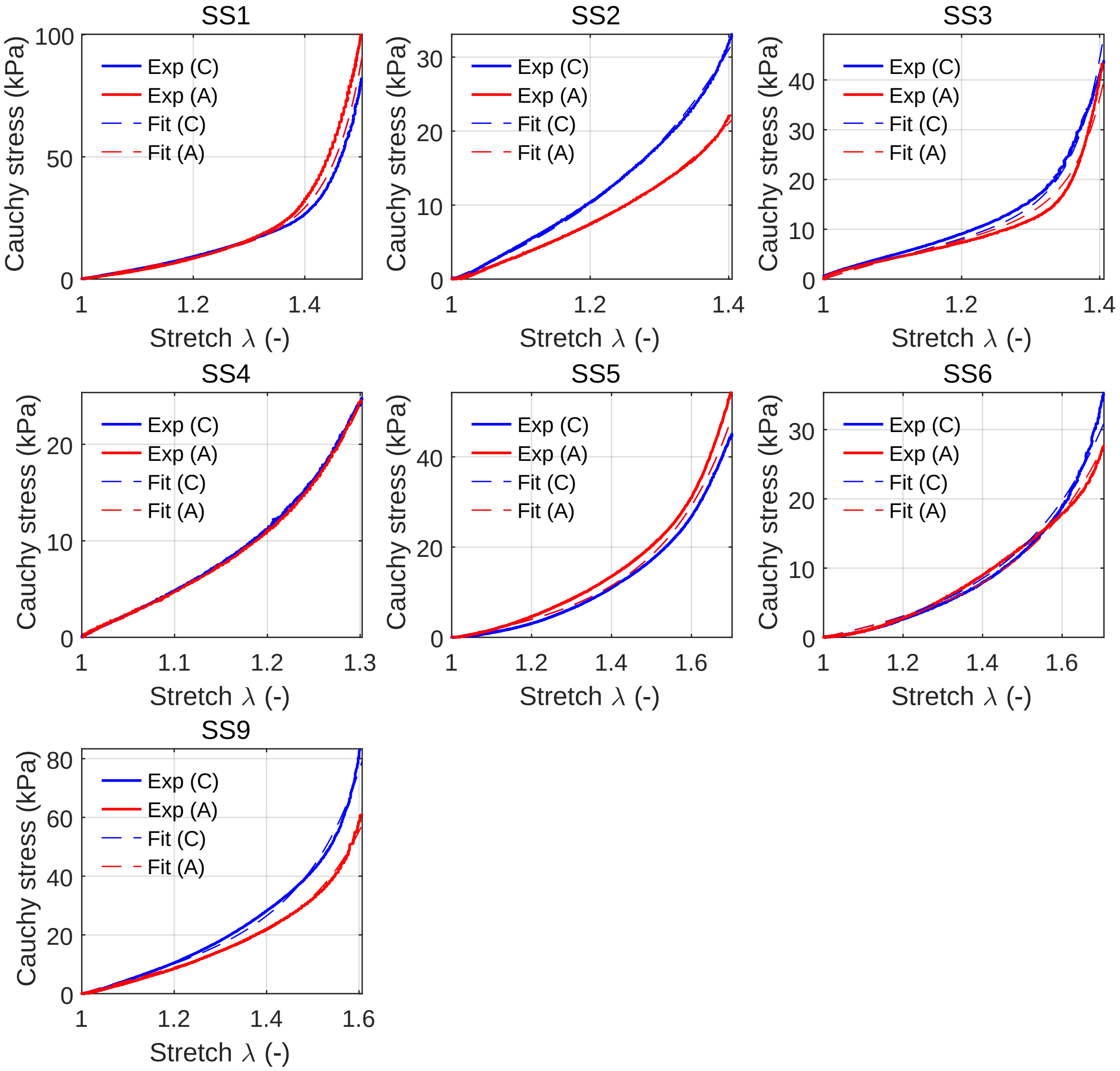

Figure 22: Parameter identification of Holzapfel-Gasser-Ogden model for sheep main pulmonary artery. The plots show the comparison between experiments and results from parameter identification obtained with MATLAB (C: Circumferential; A: Axial).

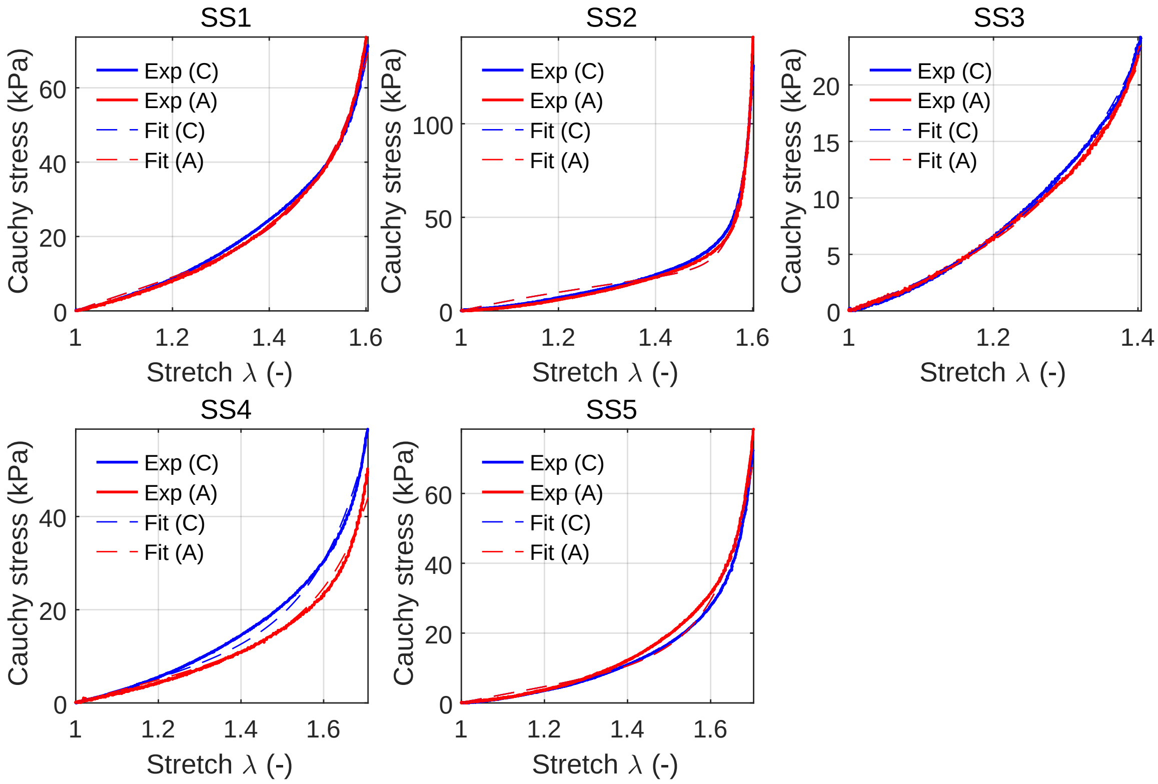

Figure 23: Parameter identification of Holzapfel-Gasser-Ogden model for sheep left pulmonary artery. The plots show the comparison between experiments and results from parameter identification obtained with MATLAB (C: Circumferential; A: Axial).

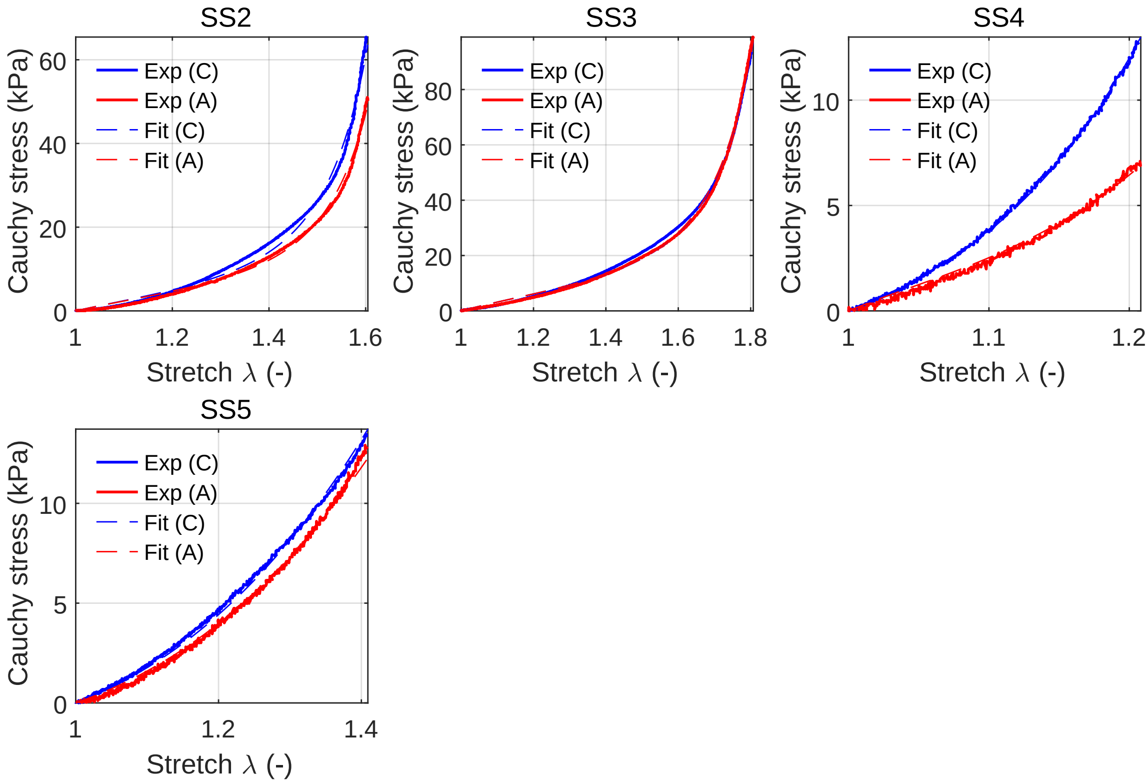

Figure 24: Parameter identification of Holzapfel-Gasser-Ogden model for sheep right pulmonary artery. The plots show the comparison between experiments and results from parameter identification obtained with MATLAB (C: Circumferential; A: Axial).

Supplementary material - Parameter identification (human)

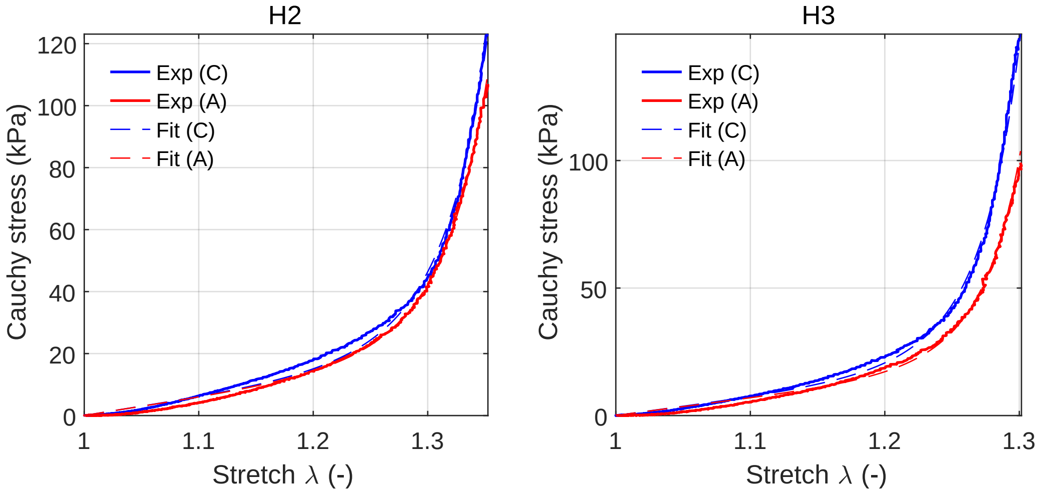

Figure 25: Parameter identification of Holzapfel-Gasser-Ogden model for human ascending aorta. The plots show the comparison between experiments and results from parameter identification obtained with MATLAB (C: Circumferential; A: Axial).

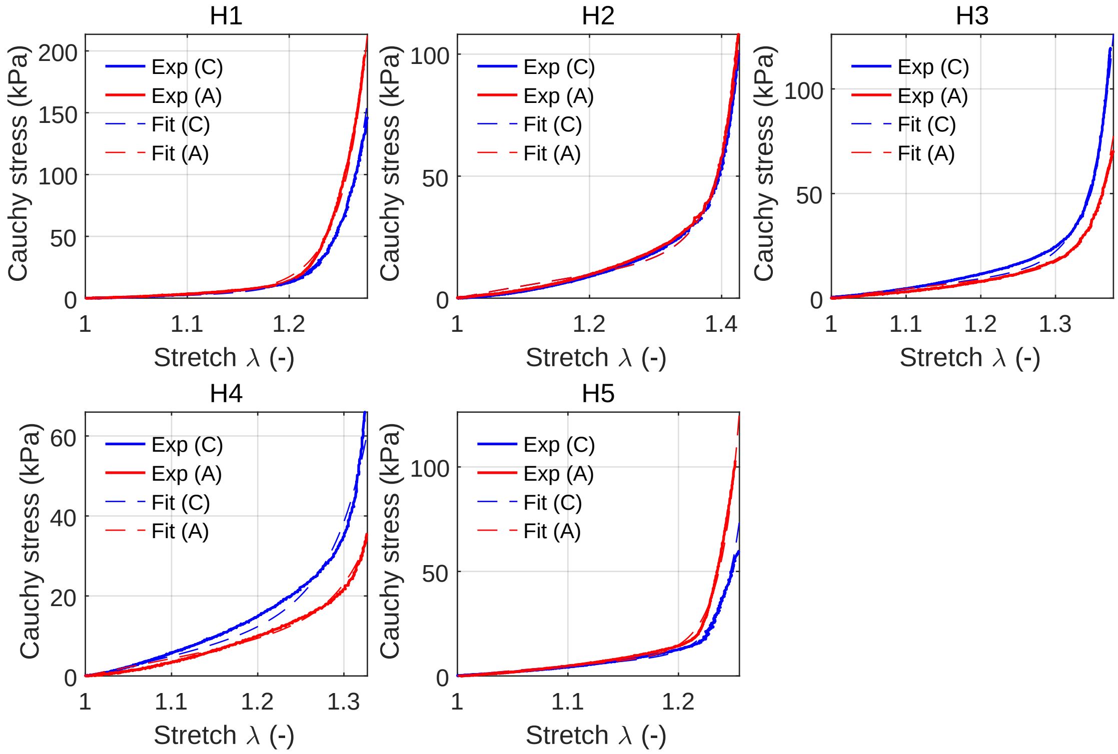

Figure 26: Parameter identification of Holzapfel-Gasser-Ogden model for human main pulmonary artery. The plots show the comparison between experiments and results from parameter identification obtained with MATLAB (C: Circumferential; A: Axial).

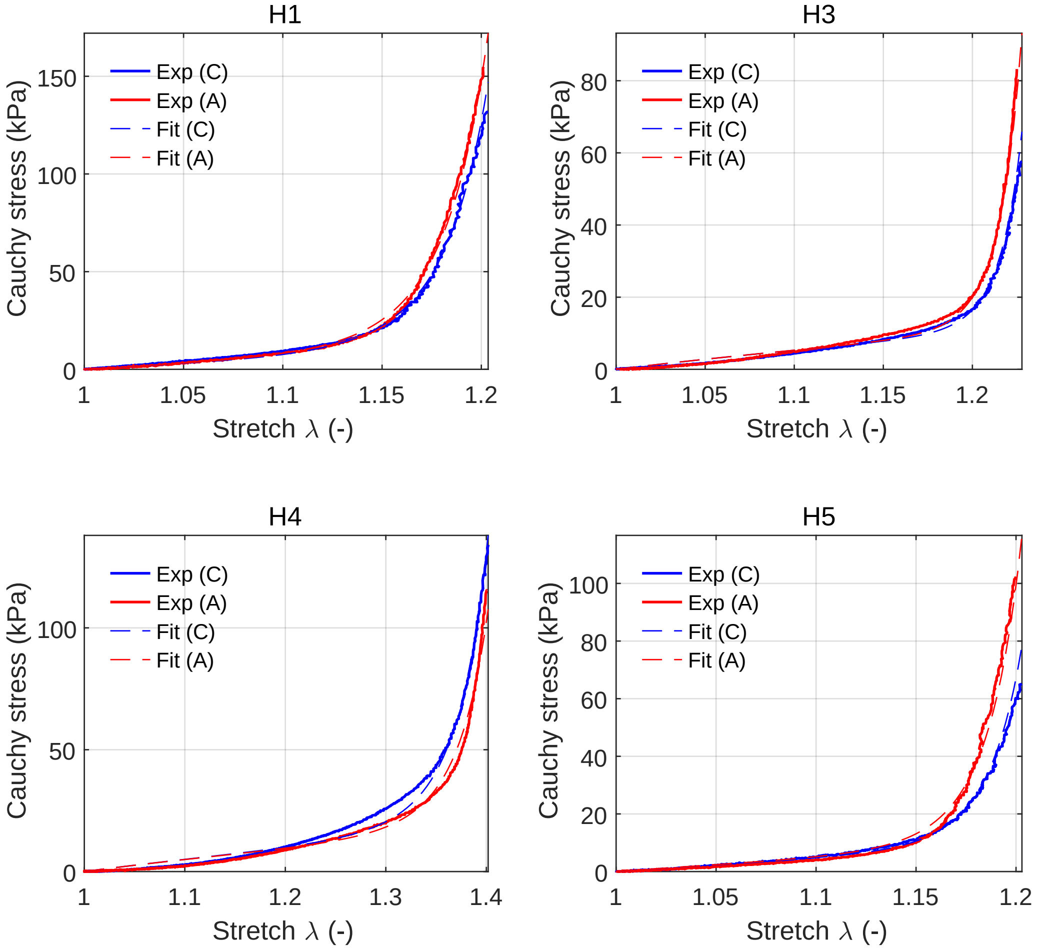

Figure 27: Parameter identification of Holzapfel-Gasser-Ogden model for human left pulmonary artery. The plots show the comparison between experiments and results from parameter identification obtained with MATLAB (C: Circumferential; A: Axial).

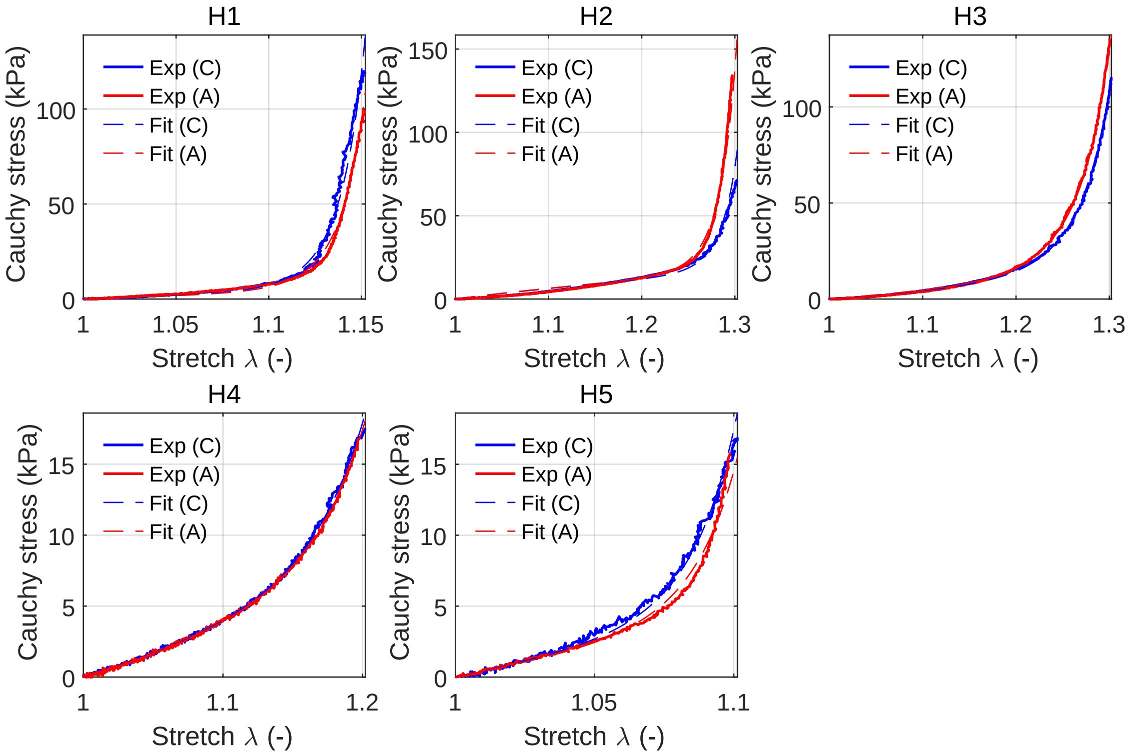

Figure 28: Parameter identification of Holzapfel-Gasser-Ogden model for human right pulmonary artery. The plots show the comparison between experiments and results from parameter identification obtained with MATLAB (C: Circumferential; A: Axial).